Review

Vasil G. Bregadze*, Tamar G. Giorgadze and Zaza G. Melikishvili

DNA and nanophotonics: original methodological approach

Abstract: The aim of the present work is a spectroscopic and thermodynamic study of DNA catalytic properties in the following processes: a) redox; b) formation of interstrand crosslinks; c) performing of photodynamic effects; d) nanoscale resonance radiationless electron excitation energy transfer. The most attention is paid to the latter, as it is truly nanoscale method in its origin. The nanoscale method of laser-induced fluorescence resonance energy transfer (FRET) to donor (acridine orange)-acceptor (ethidium bromide) intercalator pair for quantitative and qualitative study of stability quality DNA double helix in solution in real time is used. The FRET method allows to estimate the concentration of double helix areas with high quality stability applicable for intercalation in DNA after it is subjected to stress effect. It gives the opportunity to compare various types of DNAs with 1) different origins; 2) various degrees of damage; 3) being in various functional states. An alternative model and mechanisms of photodynamic effect on DNA in solutions are proposed. They are based on photoenergy degradation in solutions. The energy activates electrolytic dissociation of water molecules on H_3O^+ and OH^- and acts as a catalyst for hydrolysis reactions of phosphordiester and glycoside linkages.

Keywords: DNA; nanophotonics; nanoscale fluorescent probing of stressed DNA; photodynamic effect; resonance energy transfer.

DOI 10.1515/ntrev-2014-0021
Received May 2, 2014; accepted August 13, 2014

***Corresponding author: Vasil G. Bregadze,** Andronikashvili Institute of Physics, Department of Biological System Physics, Javakhishvili Tbilisi State University, Tbilisi, Georgia, e-mail: vbregadze@gmail.com; v.bregadze@aiphysics.ge
Tamar G. Giorgadze: Andronikashvili Institute of Physics, Department of Biological System Physics, Javakhishvili Tbilisi State University, Tbilisi, Georgia
Zaza G. Melikishvili: Chavchanidze Institute of Cybernetics, Department of Coherent Optics and Electronics, Georgian Technical University, Tbilisi, Georgia

1 Introduction

Bionanophotonics is a recently emerged, but already well-defined, truly interdisciplinary field of science and technology aimed at establishing and using the peculiar properties of light and nanoscale light-matter interaction with an emphasis on life science applications [1–9].

The deoxyribonucleic acid (DNA) molecule is well known as the blueprint of life, amazingly rich in information content and very robust. However, its unique structural features and powerful recognition capabilities can also be of interest for assembling artificial structures for a variety of applications in nanophotonics. A DNA helix is, itself, a nanoobject that can be manipulated in various ways, but it can also be treated as a versatile molecular scaffold for building nanoscale devices from the bottom up [1]. DNA's unique properties are intensively studied from different points of view: as a molecular wire, as a drug delivery system, as a ladder for ordered arrangements of various nanostructures, as a spacer to control distances between nanoobjects, etc.

Recently there is tendency in modern medicine to use such nanoscale interactions, as so-called fluorescence resonance energy transfer (FRET) in the donor-acceptor pair of dye molecules, which intensely absorb light in the visible regions of spectrum and have significant quantum yield [10–15]. Microscopic FRET is also used for cytological diagnosis of tumors [16–19].

On the other hand, there are nearly no works where quantitative estimation of FRET applied to DNA are given. For instance, energy transfer (ET) effectiveness, quantitative estimation of DNA double helix conditions, accessibility of nuclear DNA to intercalator, etc. have not been yet estimated. In this regard, it is to date the modeling of DNA defects in solution and estimation of the quality of double helix that has been investigated. It is interesting to study stress impacts on the DNA by transitive metal (TM) ions, laser irradiation, and heating.

The aim of the present work is to look at the DNA double helix's application to: 1) double proton transfer

in GC and AT pairs; 2) mobile adsorption of H_3O^+ ions; 3) inner mobility including intercalation; 4) formation of densely packed regular structure suitable for light re-emission for spectroscopic and thermodynamic study of DNA catalytic properties in the following processes: a) redox; b) nanoscale resonance radiationless electron excitation energy transfer; c) formation of interstrand crosslinks; d) performing of photodynamic effects; e) photoinduced conformation transfers in silver nanoparticles and making structures that have plasmon characteristics.

1.1 Inner mobility of DNA

Comprehensive data on the inner mobility of DNA are presented in [20]. Table 1 presents some characteristics of the inner mobility of DNA and RNA. By comparing these movements with their thermodynamic characteristics, a certain correlation can be observed. We can predict that for the excitation of a small amplitude of atom mobility, application of thermal energy is sufficient, but B→A and B→Z transition excitation requires a change in its surroundings (humidity, ionic strength, alcohols, transition metal ions, etc.). Thus, for modeling DNA structural changes, stimulated by the interactions with various ligands, particularly, metal ions (M^{2+}), it is necessary to estimate the correlation between the energy of interaction and the lifetime of such complexes, on the one hand, and dynamic characteristics of DNA, on the other.

1.2 DNA polyelectrolyte characteristics

Electrostatic potential (EP) is an additional property of metal ions, metal atoms, and nanoparticles at interactions with DNA. It depends on the composition and sequence of nucleotides and the concentration of counterions. For instance, the sequence polarity of G–C pair arrangement is-- +(N_7.O_6····HN_4), and for C–G pair, it is +--(N_4H····O_6.N_7). The pairs A–T (N_7HN_6····O_4) and T–A (O_4····HN_6.N_7) have similar arrangement -+-[23]. Quantum chemical evaluations show [24, 25] an identical sequence for the electron-donor atom arrangement both for the unscreened B-DNA form and for the one screened by Na^+ ions:

$$N_7G\text{-}N_3G\text{-}N_3A\text{-}O_2T\text{-}O_6G\text{-}N_7A$$

At first sight, DNA macromolecules are highly charged poly-anions ($2e^-$ charge per a pair of its base). Actually, according to Manning [26], at ionic strength 10^{-2}, about 76% of phosphate groups are in a complex with Na^+ ions (pK~3). It means that for the Na^+ ions adsorbed stated in accordance with expression 3 (see Section 1.4), the lifetime of DNA-Na^+ complex is ~10^{-8} s. It, in its turn, facilitates the interaction of transition metal ions, atoms, and small nanoparticles with electron-donor atoms located in major grooves of the DNA double helix. On the other hand, negatively charged phosphate groups and counterions (mobile ions) lead to the formation of hydrodynamic layers near the DNA surface. Thus, the DNA sites with condensed Na^+ ions and the sites surrounded by hydrodynamic layers

Table 1 Characteristics of inner movements in DNA.

Type of movement	Time (s)	Excitation energy (kcal/mol)
1. Various small-amplitude oscillating movements of atoms (about 0.1 Å) inside the components of DNA	10^{-14}–10^{-13} (3500–300 cm^{-1})	RT(T=300 K)=0.6(210 cm^{-1})
2. Limited movements of phosphates, sugars, and nucleobases relative to the equilibrium position, torsional, and flexural oscillations of the double helix	10^{-10}–10^{-8}	
3. Large-amplitude movements of phosphates, sugars, and bases occurring in connection with the transition of the double helix from one form to another	10^{-7}–10^{-5}	5–6 for B→A transitions and 21 for B→Z transitions [21]
4. Change of free energy ΔG needed for opening of central pairs in double chain RNA at 298 K, kcal/mol bases [22]		
GC 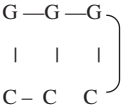 and	~3×10^{-6}[a]	7.5
AU 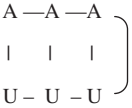	~10^{-8}[a]	4.0

[a]The time of pair opening is evaluated by expression (3).

(water and mobile counterions) will be in dynamic equilibrium. So transition metal ions such as Mn(II), Co(II), Ni(II), Zn(II), and Cu(II) not only form outer sphere complexes with DNA but also form outer interchain crosslinks with the DNA double helix. At the same time, Cu(I) and Ag(I) ions form inner sphere complexes with the DNA, particularly chelate N_7G-O_6G complex and interstrand N_1G-M(I)-N_3C crosslinks. Special attention should be paid to H^+ because H^+ ions are the exception, and they are characterized by the mobile-adsorption state on the DNA surface. It is demonstrated by 1) an abnormally strong effect of H^+ ions on the DNA spectra in the UV region and strong influence of ionic strength on the interaction between H^+ and DNA [27]; 2) weak effect of H^+ ions on DNA stability in the complex with intercalators; 3) absence of silver nanoparticles (AgNPs) oxidation in DNA complexes by H^+ ions in the presence of Ag(I) or Cu(II) ions; 4) abnormally high mobility of H^+ ions (lifetime 10^{-13} s in water and 10^{-14} s in ice [28]).

1.3 Intercalation

One more interesting characteristic of DNA is intercalation. Intercalator binding coefficients with natural DNA and model nucleotides is between the 10^4 and 10^6 sequence. Such a type of molecule intercalator binding with the DNA double helix takes place, as a rule, in two steps. The first step is adsorption of intercalators on periphery areas of the surface; at the second step, the intercalators penetrate into the DNA molecule, which is accompanied by unfolding and elongation of the helix and, certainly, by increasing the helix rigidity. The first step is characterized by weak binding. Binding constants given above are typical for intercalation processes. Besides, the intercalation process is characterized by the principal of excluding the nearest binding places. In the case of proflavine, only 44% of possible binding places are busy [29]. It means that every second place is vacant. But there are some data that allow doubt in the statement. In particular, our group has managed to obtain fluorescence spectra of the DNA ternary complex DNA-AO-EB at a specific concentration of three intercalator molecules to 5 base pairs (bp) of DNA (see Figure 1). It should be underlined that unlike soft ions such as Ag(I), ions of Ni(II), Co(II), Zn(II), Mn(II), Cu(II) choose stable nucleotide dimmers. Intercalators when binding with DNA prefer the same dimmers. For instance, overlapping is much stronger in the sequence pyrimidine – 3′, 5′ – purine than at the intercalation of sequence purine – 3′, 5′ – pyrimidine. It means that, in the first case, the energy gain is 29–54 kJ/mol more than in the second case [31].

1.4 Adsorbing thermodynamic model of DNA interaction with small ligands

Metal-induced catalytic characteristics of DNA are closely related to the modeling of its structural changes caused by interaction with different ligands, such as metal ions, in particular. Thus, for modeling structural changes of DNA, stimulated by the interaction with ligands or metal ions (M^{2+}), it is necessary to know the correlation between the energy of the interaction and the lifetime of such complexes, on the one hand, and the dynamic characteristics of DNA on the other. It can be concluded that a local influence of transition metal ions on structural changes in DNA is possible only in case when the lifetimes of the complexes are commensurable to the specific times of inner mobility in DNA (oscillation of small groups of atoms, double helix untwisting, opening of the individual base pairs, untwisting of helix binding of proteins and cell division). The movements last from 10^{-10} s to hundreds of seconds and longer. We have managed to find such a correlation [32], by applying Frenkel's phenomenological thermodynamic approach [33–35], which was used as early as 1924 for the study of gas adsorption by the surface of solid bodies. Frenkel introduced a new term "lifetime" for adsorption state τ and connected it to the energy of interaction $|\Delta E|$ between adsorbate and adsorbent surface by the following expression:

$$\tau = \tau_0^{a\text{-}s} \cdot \exp(\Delta E / k_B T) \quad (1)$$

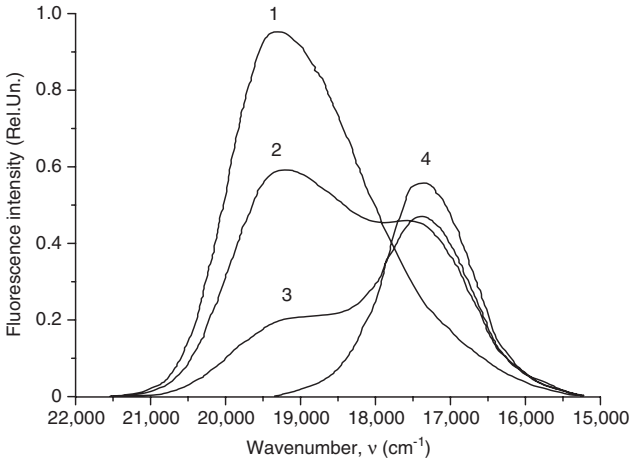

Figure 1 Fluorescence spectra of ternary complex DNA-AO-EB. [AO]-3×10^{-5} mol/l, [EB]-0 mol/l (1); [AO]-2×10^{-5} mol/l, [EB]-1.0×10^{-5} mol/l (2); [AO]-1.5×10^{-5} mol/l, [EB]-1.5×10^{-5} mol/l (3); [AO]-1×10^{-5} mol/l, [EB]=2×10^{-5} mol/l (4). [DNA]-10^{-4} mol/l (P), [NaCl]-0.01 mol/l, pH7 [30].

where $\tau_0^{a\text{-}s}$ is a single oscillation time of the adsorbate relative to the surface, which is assumed to be 10^{-13}–10^{-12} s; k_B is the Boltzmann constant.

In good approximation to the above model is the study of small ligand interactions with biomacromolecules in solutions, and indeed, using the relation of equilibrium constant K for ligand-biopolymer reactions with the change of Gibbs' free energy ΔG, we get

$$\Delta G = -RT\ln K, \tag{2}$$

where R is the gas constant (8.31446 J/mol·K), T is the absolute temperature of substance. We have obtained the final expression for the description of time for small ligand interaction with macromolecules

$$\tau = \tau_0 \cdot K, \tag{3}$$

where τ is the lifetime of ligand-macromolecule complexes. Now, we must clarify the value τ_0 for solutions. Frenkel's $\tau_0^{a\text{-}s}$ is the duration of the fluctuation excitation of adsorbing atoms or molecules interacting with a solid surface, and it is supposed to be equal to the period of the oscillation of adsorbate relative to the adsorbent surface. In solutions, the value τ_0 describes the duration of the relaxation of rotary and translation movements of the solvent molecules, ions, solvated ions or low molecular weight substances and lies between 10^{-11} and 10^{-10} s. Thus, if we assume that $\log K = 4$–6 for DNA binding with twofold positively charged metal ions of the first transition series, and $\tau_0 = 10^{-11}$ s, then the life span of these complexes is about 10^{-7}–10^{-5} s.

So, we have managed to correlate the stability constant for the complex formation K, which can be registered in the equilibrium state, to dynamic characteristic τ for the lifetime of a complex. Thus, the principal concept of molecular biophysics regarding biomolecules: structure-dynamics-function can be reformulated as structure-stability-function. It should be specially noted that such an approach highly simplifies and widens the time interval (from 10^{-10} s to 10^5–10^6 s and more) under the investigation of dynamic characteristics of macromolecules.

Derivation of formulae (3) and its detailed ground are given in [32].

2 DNA as catalyst in redox reactions

2.1 Oxidation

Figure 2 shows the absorption spectra for AgNPs and AgNPs-DNA complexes. Figure 3 presents first derivatives of absorption spectra for AgNPs and AgNPs in the complex with the DNA.

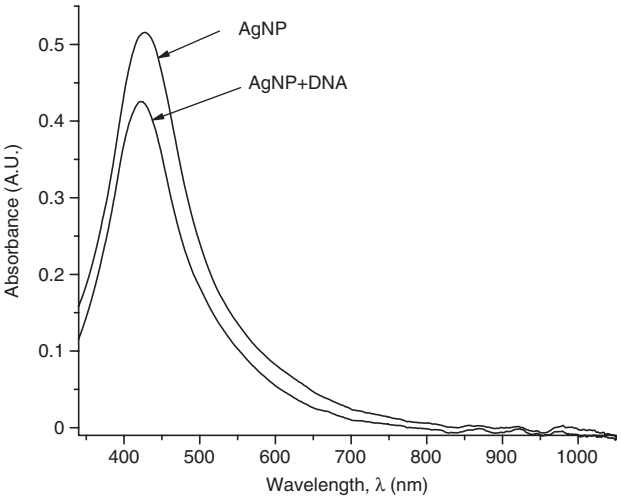

Figure 2 Absorption spectra of AgNPs and AgNPs-DNA complexes. [AgNPs] – 0.72×10^{-4} mol/l (Ag^0), [DNA] – 1.6×10^{-4} mol/l (P), [$NaNO_3$] – 10^{-2} mol/l.

The analysis of Figures 2 and 3 shows that at DNA interaction with AgNPs, a short-wave shift of AgNPs absorption band (6 nm) takes place. Besides, a 20% hypochromic effect can be observed.

It should be pointed out that the values of the hypsochromic shift and hypochromic effects depend to a certain extent on the lifetime of AgNPs. A distinct trend is observed in the decrease of these effects connected with time. The short-wave shift points out that at the interaction with DNA, there is a kind of loosening of the interaction

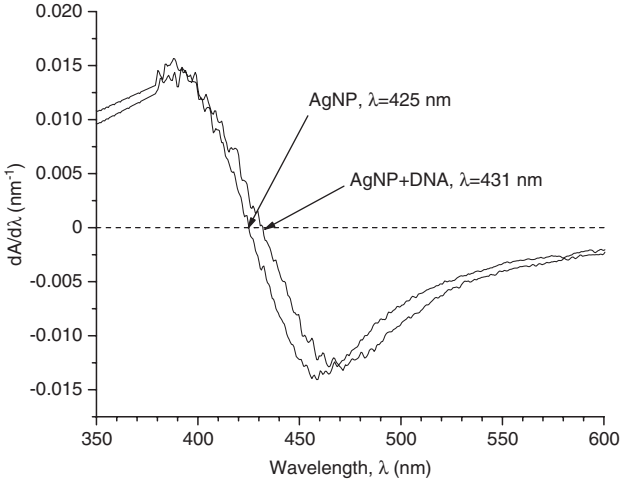

Figure 3 First derivative of absorption spectra of AgNPs and AgNPs-DNA. The blue shift is evident.

between the silver atoms inside the AgNPs. The decrease in the intensity of the absorption band is due to the partial corrosion of AgNPs in the presence of DNA. At DNA interaction with AgNPs and H_3O^+ in water solutions, AgNPs-DNA and H_3O^+-DNA complexes are formed. H_3O^+ ions being in a mobile adsorbed state on the surface of DNA [32, 36] can form complexes with AgNPs. Nanoparticles, in turn, moisturize the DNA surface. We have not found any data on O_2 and NO_3^- molecule adsorption on the DNA surface, though high concentrations of NO_3^- (0.3 mol/l) can oxidize AgNPs (see Figures 4 and 5). Photo-irradiation in water also oxidizes AgNPs [37].

As early as 1980 [38], one of the authors of the present work proposed a definition of various ion and molecule affinity to electrons in water solutions as reciprocal to the activation energy ΔGa of a hydrated electron (e^-_{aq}) with organic and inorganic substances in the water solution rate constant which is evaluated as $k_{e\text{-/aq}}=10^{11}\exp(-\Delta Ga/RT)$ [39]. Taking as an example the study of DNA interaction with transition metal ions by absorption spectrometry and equilibrium dialyses, we have shown that as a rule, the bigger is $K_{e\text{-/aq}}$ value for the metal ions, the more intensive is their interaction with DNA [39].

Table 2 shows rate constants $k_{e\text{-/aq}}$ and $1/\Delta Ga$ for the reaction with Ag^+, H_3O^+, NO_3^- ions and O_2, H_2O, and DNA molecules, where ΔGa is the hydrated electron activation energy according to $k_{e\text{-/aq}}=10^{11}\exp(-\Delta Ga/RT)$. Besides, in the last column of Table 2, the concentration of the substances under investigation is given.

It can be explained by the ability of DNA to adsorb H_3O^+ (pK~4) and metal ions of the first transition row M^{2+} (pK=4-6) [40]. It should be noted that in the study of

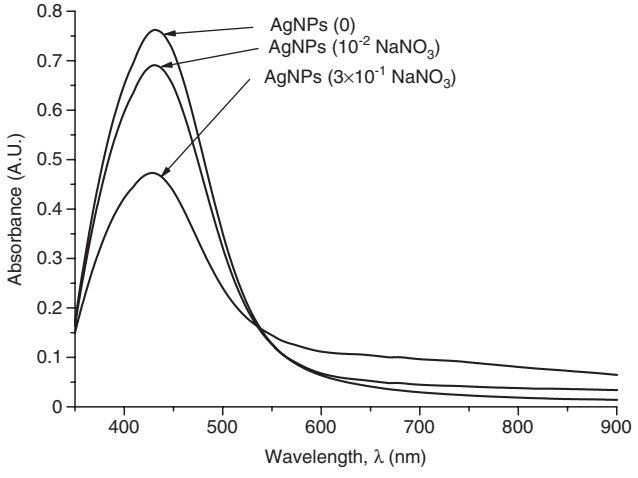

Figure 4 Absorption spectra of AgNPs after various ion strength applications. [AgNPs] – 0.7×10^{-4} mol/l (Ag^0), [$NaNO_3$] – 10^{-2} mol/l (C_1); [$NaNO_3$] – 3×10^{-1} mol/l (C_2).

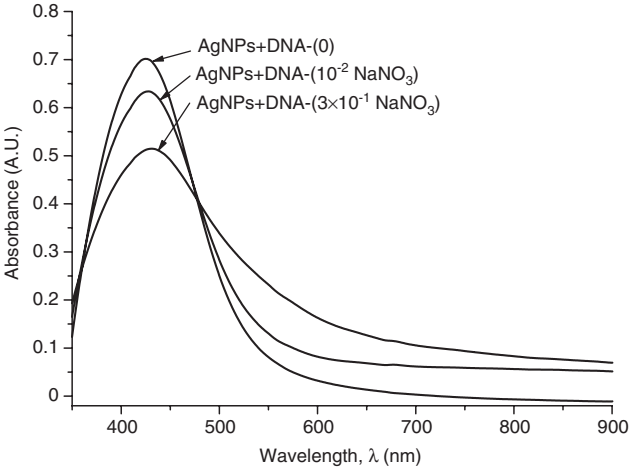

Figure 5 Absorption spectra of AgNPs and DNA after various ion strength applications. [AgNPs] – 0.7×10^{-4} mol/l (Ag^0), [DNA] – 1.8×10^{-4} mol/l (P), [$NaNO_3$] – 10^{-2} mol/l (C_1); [$NaNO_3$] – 3×10^{-1} mol/l (C_2).

the interaction of transition metal ions with DNA, non-buffer solutions are usually used. As a rule, the pH of the solutions is 5.5–6. At these pH values, the concentration of H_3O^+ in the solution is satisfactory for the attacks at DNA because H_3O^+ adsorption on DNA is of a mobile character [36]. Thus, the surface of DNA can adsorb both AgNPs and H_3O^+ and serves as a catalyst in the AgNP oxidation reaction. So, we can state with definite certainty that in AgNPs-H_3O^+ complexes, which exist on the DNA surface, electron transfer from the silver atom to H_3O^+ can occur because the value of electro-negativity of hydrogen atom is bigger than that of the silver atom and much more than that of the H_3O^+ ion. We can express it by the following equation:

$$2\,\mathrm{AgNPs(n)}+2\mathrm{H}^+\rightarrow 2\,\mathrm{AgNPs(n\text{-}1)}+(2\,\mathrm{AgNPs}+\mathrm{DNA})+\mathrm{H}_2\uparrow$$

It is necessary to underline that AgNPs used in the experiment have the size of 1–2 nm, and consequently,

Table 2 Values for reaction rate constants of hydrated with Ag^+, H_3O^+, NO_3^- ions, and O_2, H_2O and DNA molecules.

Ions and molecules	pH	$k_{e/aq}$ ($mol^{-1}\,s^{-1}$)	ΔGa^{-1} (mol/kcal)	Concentration in solution (mol/l)
Ag^+	7	3.2×10^{10}	1.468	1.1×10^{-4}
AgNPs	6	–	–	0.74×10^{-4} (Ag^0)
H_3O^+	4-5	2.36×10^{10}	1.157	0.3×10^{-4}
NO_3^-	7	1.1×10^{10}	0.757	10^{-2}
H_20	8.4	1.6×10^{1}	0.074	–
Na^+	7	$<10^5$	0.121	0.8×10^{-4}
O_2	7	1.88×10^{10}	1	1.33×10^{-6}
DNA	7	~10^8	0.242	$2\cdot10^{-4}$ (P)

their concentration is at least two orders less than the one for atoms, which constitute the particles. Assuming that all nanoparticles of the solution are adsorbed on the DNA, and they interact from the side of the double helix major groove, and their average size is 1.5 nm, we can conclude that the average distance between AgNPs adsorbed on the DNA is nearly 60 nm (one particle for about 170 bp). As soon as H_3O^+ reduction starts (as a result of AgNPs oxidation), the water in the solution dissociates to OH^- and H^+ supplying new H_3O^+ until a new dynamic balance of the system is achieved. Ag^+ ions, which are created during the reaction, have a high stability constant with DNA (pK≥10.8 [36]). As early as 1969, Wilhelm and Daune [41] showed that Ag^+ ions make two kinds of intra-spherical complexes with G-C DNA pairs: chelate N_7G-O_6G and intrastrand linear complex between N_1G and N_3C, the so-called crosslink. The authors [41] believe that in making the complex of the second type, H_3O^+ is released from the DNA guanine into the solution. It is an additional mechanism of H_3O^+ formation in solution. As formation of the second type of complex depends on the DNA dynamic characteristics, i.e., on the frequency of unfolding the base pairs, the possibility of the process will be much higher in case when DNA is denatured. We could observe it in our experiment.

2.2 Reduction

Figure 6 demonstrates the absorption spectra of AgNPs and of the following complexes DNA-$AgNO_3$-AgNPs, DNA-$AgNO_3$-AgNPs-AA. In contrast to the spectra shown in Figure 7, the absorption spectra of quaternary complex DNA-$AgNO_3$-AgNPs-AA have greater intensity and different places for absorption maximums. It can be seen that ascorbic acid (AA) reduced silver ions in ternary complex DNA-$AgNO_3$-AgNPs. Thus, AgNPs activate the process of quick reduction of Ag^+ ions to silver atoms. Analyzing the absorption spectra given in Figure 6, we can draw the following conclusions: 1) Ag^+ ions interfere in H_3O^+ ion mobility and prevent oxidation of AgNPs and 2) AgNPs, in turn, activate the process of Ag^+ ion reduction in the presence of AA. The AgNP absorption spectra shift to the red side (6–7 nm), and significant increase in the absorption spectra intensity undoubtedly point out the increase in AgNPs size in the complex with DNA. It should be underlined that, without DNA, nothing happens to AgNPs in water solution.

Figure 7 presents the AA effect on the absorption spectra of the DNA complex with silver ions in the visible region. By 160 min, we can clearly see the appearance of

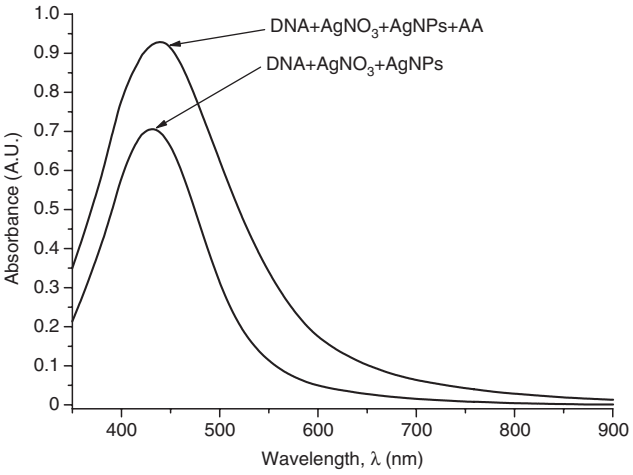

Figure 6 Absorption spectra of AgNPs and the following complexes DNA-$AgNO_3$-AgNPs and DNA-$AgNO_3$-AgNPs-AA. [AgNPs] – 0.7×10^{-4} mol/l (Ag^0), [DNA] – 1.8×10^{-4} mol/l (P), [$AgNO_3$] – 0.7×10^{-4} mol/l, [AA] – 1.4×10^{-4} mol/l, [$NaNO_3$] – 10^{-2} mol/l.

a notable spectrum from the reduction of silver atoms. In 24 h, the absorption spectra specific for silver atoms can be observed. It is seen that the absorption spectra have a complex form, they are reminiscent of the absorption spectra of substances having specific resonance interactions. Resonance interactions are specific for structures having identical chromophore and hard structure [42], e.g., for the absorption spectra of poly-peptide in the α-helix state [43]. Interaction of silver ions, which is characterized by inter-cross type of links with DNA, reduces dynamic characteristics of double helix and makes it harder. The other reason for the complexity of the spectra is the reduction of silver ions and their further

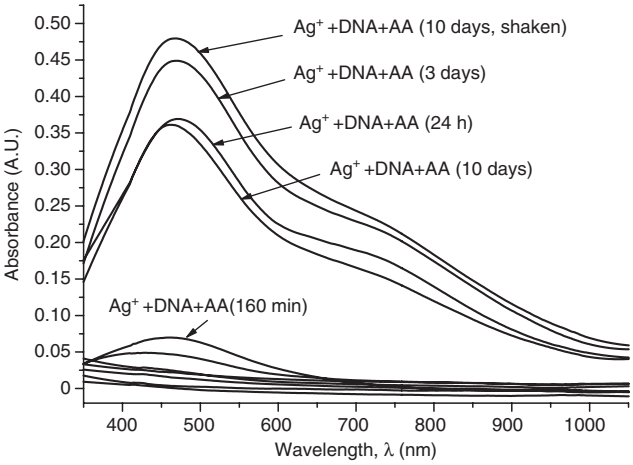

Figure 7 Spectra for silver ion reduction in complexes. DNA-$AgNO_3$-AA. [DNA] – 5.9×10^{-4} mol/l (P), [$AgNO_3$] – 1.2×10^{-4} mol/l, [AA] – 2.4×10^{-4} mol/l, [$NaNO_3$] – 10^{-2} mol/l.

condensation in clusters and nanoparticles with the size of more than 50 nm [44].

3 Photo-induced DNA-dependent conformational changes in AgNPs

Figure 8 shows the AgNP absorption spectra before and after their heating followed by their cooling. Colloidal silver suspension was placed in a hermetic test tube, and it was incubated in a vessel with boiling water for 15 min. Then, the test tube with the sample was cooled in an ice bath to room temperature. It can be seen from Figure 8 that nanoparticles exposed to heating demonstrate noticeable weakening of absorption intensity, and what is very important is the widening of absorption spectra from 140 nm to 215 nm.

Hypsochromic shift and widening of the AgNP absorption spectra caused by their interaction with DNA and heating demonstrates, on the one hand, loosening of AgNPs, i.e., penetration of solvent in nanoparticles, the atoms of which show weaker polarizability than water [45, 46].

The company NanoComposix [44, 47] gives sample absorption spectra for spherical AgNPs with particle sizes of 10, 20, 30, 40, 50, 60, 70, 80, 90, and 100 nm at the same mass concentration 0.02 mg/ml. The given data show that with the increase in the size of the particles, widening

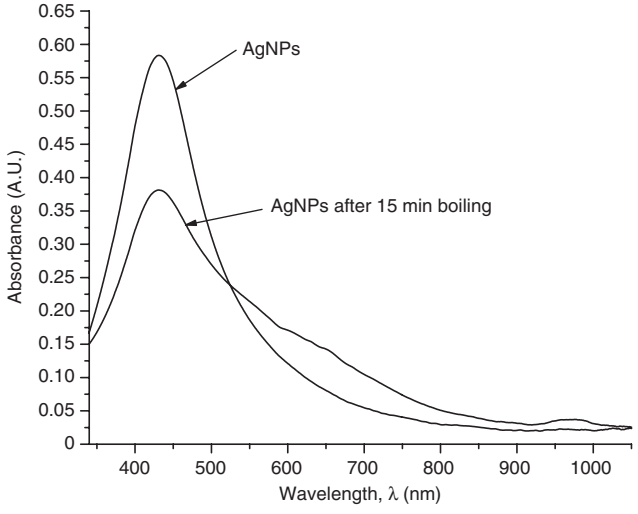

Figure 8 Absorption spectra of AgNPs before (1) and after (2) heating (15 min incubation at T=373 K) [AgNPs] – 0.72×10^{-4} mol/l (Ag^0), [$NaNO_3$] – 10^{-2} mol/l.

of the red shift of the absorption band can be observed. It is notable that despite the growth of the particle size, i.e., decrease in their total number in the solution, the intensity of the absorption bands for nanoparticles with the sizes from 10 to 40 nm is not practically changed, only a small shift of absorption band maximums can be observed. The above explicitly points out that chromophore units are silver atoms and not nanoparticles. Thus, we can draw a conclusion that silver atoms in AgNPs are sufficiently isolated and bound together by dispersion interaction (induced dipole-induced dipole). As these interactions are performed in the surrounding water, they should be considerably amplified at the expense of the so-called hydrophobic effect [48], which means compaction and then minimization of the surface (decrease of the system entropy).

We should especially point out that in a nanoparticle, which consists of one kind of atoms, along with the mentioned dispersion interaction, the so-called resonance interaction should take place [42]. Such types of interactions are typical for molecular crystals, and they usually lead to exciton splitting of the principal absorption band. Inevitable condition for exciton splitting is the presence of a system consisting of identical groups and having a hard structure [43]. The absence of splitting can mean that AgNPs under investigation (Figure 2) have a liquid structure resembling a drop, which under definite conditions such as temperature, photo-irradiation, variations in dielectric constant of the environment should be characterized by conformational transitions. So, once again, analyzing the absorption spectra presented in Figure 2, we can make the conclusion that hypsochromic shift shows not only loosening of AgNPs, but moreover, the transfer of the drop into a spherical segment with the wetting angle $\theta<\pi/2$ (see Figure 9). It means that the DNA surface is moistened by silver nanoparticles. First of all, it is connected with great affinity of soft ions (Cu^+, Ag^+, Hg^{++}, etc.) and metal ions M^0 with the DNA double helix [36]. Photo-diffusion of AgNPs (see Figure 10) on the DNA double helix resembles flesh-desorption phenomena, i.e., fast heating of AgNPs by photons, then desorption of silver ions with their following adsorption by DNA double helix, including creation of crosslinks between silver atoms and DNA chains.

The kinetics of AgNP photoirradiation has also been studied. Figures 10 and 11 show superposed absorption spectra of free AgNPs and AgNPs in complex with DNA before and after irradiation using a water filter.

The analysis of the spectra in Figures 10 and 11 demonstrates that only the irradiated complexes AgNPs-DNA have distinctly expressed isosbestic point. The test with

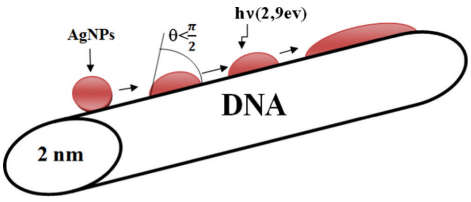

Figure 9 Model of DNA moisturizing by silver nanoparticles.

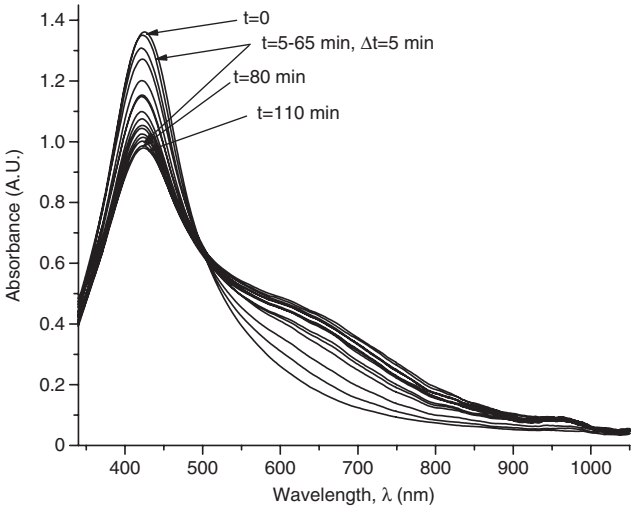

Figure 10 Absorption spectra of AgNPs-DNA before and after irradiation (5-min interval). [AgNPs] – 1.94×10^{-4} mol/l (Ag^0), [DNA] – 1.6×10^{-4} mol/l (P), [$NaNO_3$] – 10^{-2} mol/l.

the free AgNPs shows that, as a result of photoirradiation, desorption of silver atoms and their oxidation to Ag^+ ions takes place. The presence of isosbestic points

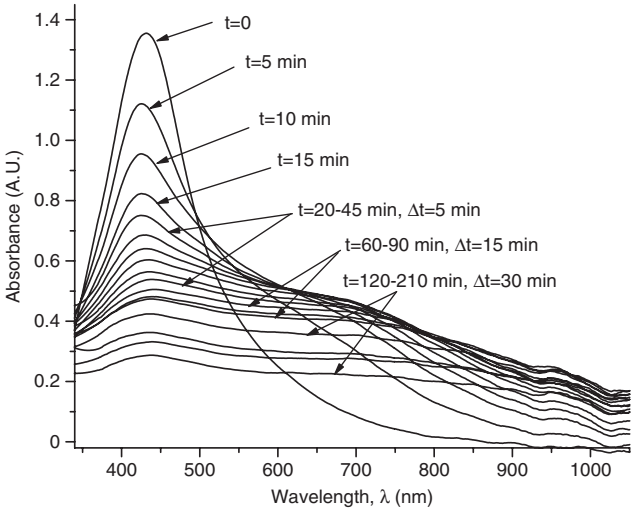

Figure 11 Absorption spectra of AgNPs before and after irradiation (5-min interval). [AgNPs] – 1.94×10^{-4} mol/l (Ag^0), [$NaNO_3$] – 10^{-2} mol/l.

in the absorption spectra of irradiated AgNPs-DNA complexes proves that the system has no less than two states, i.e., AgNPs-DNA complexes have several forms of existence joint by structural photodiffusive transition from one form, e.g., spherical one, to an extended long, and probably one-dimensional form along the DNA double helix. The analysis of the spectra really shows with good correlation (≤5%) that the space under the spectra is preserved, which means that there are no changes in the chromophore electron structure. Besides, half the width of the absorption spectra $\Delta\lambda_{1/2}$ is changed from 140 nm to 360 mn. Red shift and widening of the AgNP absorption band points to the typical for molecular system increase of electron conjugation (linear and cyclic conjugated systems [49]).

We have also carried out the evaluation of energy needed for the heating of AgNPs (1–2 nm). Under the condition when atomic (specific) heat capacity of liquid silver is equal to 30.5 J/(g-atom×grad); single photon energy (λ=430 nm) is 46.2×10^{-20} J, it is possible to heat a single silver nanoparticle (size 1 nm) consisting of 30 silver atoms up to 610 K; in the case when a silver nanoparticle has a size of 2 nm, i.e., consists of 240 atoms, it can be heated up to 340 K. It means that photo-irradiation (λ=430 nm) has the absolute ability to cause the photodiffusion of AgNPs, especially of those with size about 1 nm.

To check the concept, we have carried out thermodynamic kinetic analysis of absorption spectra of AgNPs-DNA complexes (see Figure 10).

Let us consider the changes in absorption spectra for photo-irradiated AgNPs-DNA complexes given in Figure 10 *versus* the duration of irradiation in M_t/M_e and $t^{1/2}$ (see Figure 12). $M_e=A_{t=0}-A_{t=6600}$ is the number of silver atoms in the nanoparticles at the beginning (absorption A_t when λ=430 nm at t=0), $M_t=A_{t=0}-A_t$ is the molar quantity of silver atoms desorbed by the time moment t (difference between absorption $A_{t=0}-A_t$ at λ=430 nm). As can be seen, the curves in Figure 12 have an S-shape for photodesorption kinetics of silver atoms both from the surface of free AgNPs and AgNPs-DNA complexes. The S-shape appearance of the curves denotes that photo-induced desorption of atoms is a complex and multiphase process [37]; it means diffusion of silver atoms from the inner part of a nanoparticle to its surface, conformational changes in the particles especially in the ones that are adsorbed on the DNA surface. Next, we are going to consider the results given in Figures 10 and 11 in $\ln[M_e/(M_e-M_t)]$ and t coordinates, which are given in Figure 13.

The analysis of the curve shows that only the initial stage of the given curves of the desorption kinetics obey the linear law of Langmuir first-order equation

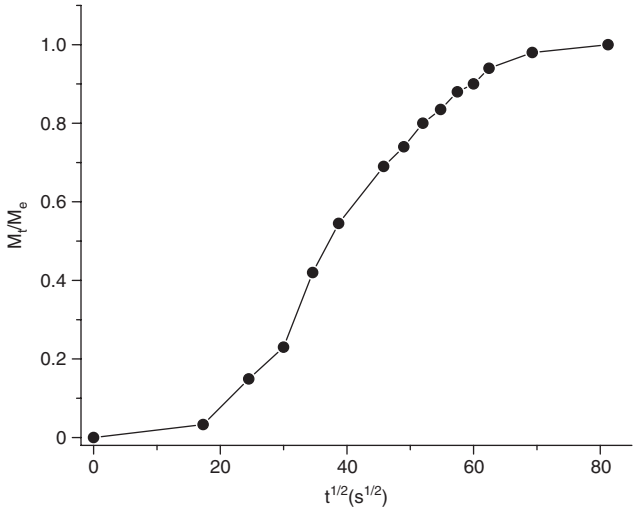

Figure 12 Kinetic curve of photo-desorption in M_t/M_e and $t^{1/2}$ coordinates for AgNPs bound with DNA.

$$\ln[M_e/(M_e\text{-}M_t)]=kt. \quad (4)$$

The constant of desorption rate for silver atoms from the surface of AgNPs has been evaluated from the slopes of the curves, and the data is, for AgNPs bound with DNA, $k_d \cong 9\times10^{-5}s^{-1}$. The values allow us to estimate the activation energy E_d for the desorption reaction using the equation

$$k_d=v_0 \exp(-E_d/RT) \quad (5)$$

where v_0 is the pre-exponential factor assumed as $v_0 \approx 10^{10}s^{-1}$ (reciprocal quantity to silver atom oscillation time in nanoparticles). In this case, we have acquired the value for $E_d \cong 80$ kJ/mol Ag^0 for AgNPs bound with DNA at T=300 K

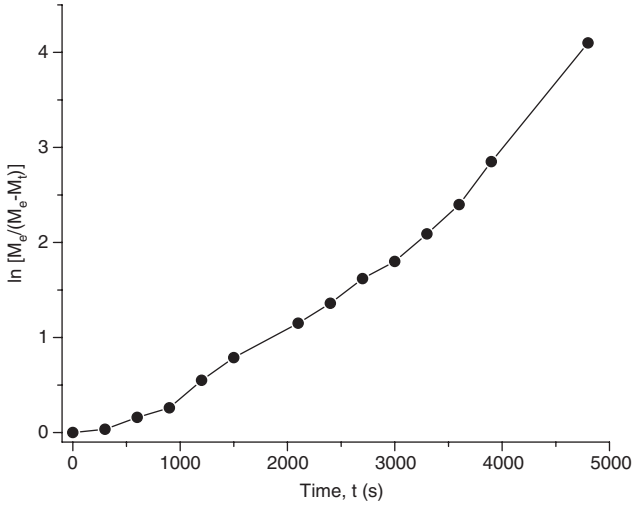

Figure 13 Kinetic curve of photodesorption in $\ln[M_e/(M_e\text{-}M_t)]$ and t coordinates for AgNPs bound with DNA.

As $E_d=E_a+Q_a$, where E_a is the adsorption activation energy, and Q_a is the adsorption heat of nanoparticles, so $Q_a \cong 80$ kJ/M Ag^0 under the condition that formation of nanoparticles is not an activated process. The value of heat is specific for cluster nanostructures [50].

Silver atom photodesorption from the surface of nanoparticles, included in the DNA complex, has a desorption activation energy of 80 kJ/mol Ag^0, and consequently, we can assume that photo-induced diffusion of AgNPs on DNA double helix takes place along with the activation of silver atom desorption energy, which equals to 80 kJ/ mol Ag^0, and thus, we can state that the energy of Ag^0 interaction with the DNA double helix is not <80 kJ/mol Ag^0. In accordance with the Gibbs equation

$$\Delta G=-RT\ln K, \quad (6)$$

and taking into account the evaluated energy 80 kJ/mol Ag^0, we assume that the stability constant of the complex is not $<10^{14}$, and consequently, the lifetime of the complexes is equal to 10^4 s. The lifetimes of 1 s order and more are characteristic for interstrand interactions with the participation of transition metal ions, so-called crosslinks [22]. As early as 1969, Wilhelm and Daune [23] showed that Ag^+ ions form crosslinks between DNA chains, thus, releasing protons bound with N1 guanine and N3 thymine into the solution. We have estimated stability constants of Cu^+ and Ag^+ ions with DNA, which are equal to pK=10.8 for Ag^+ and pK=14.9 for Cu^+. Thereafter the change of free energy for Ag^+ is 63 kJ/mol and 86 kJ/mol for Cu^+ and life times are 0.63 s for Ag^+ and 8.6×10^3 s for Cu^+ [4].

4 Nonradiative energy transfer between intercalator molecules and defects in the DNA duplex

Interaction of intercalator molecules with DNA, particularly, acridine orange (AO) and ethidium bromide (EB) (Figure 14), depends on ionic strength of the solution, DNA nucleotide content, its sequence [51], and double helix structure. Besides, such an interaction depends on transition metal ions (TM) [32], which cause ejection of intercalators, though intercalator molecules and TM ions have different binding sites on DNA. We should point out that AO and EB molecules as well as TM ions [Mn(II), Co(II), Ni(II), Cu(II), and Zn(II)] at the interaction with the DNA double helix have similar values of stability constants, and their pK are in the 4–6 interval [51]. At the interaction with DNA, TM ions provoke point defects such as double

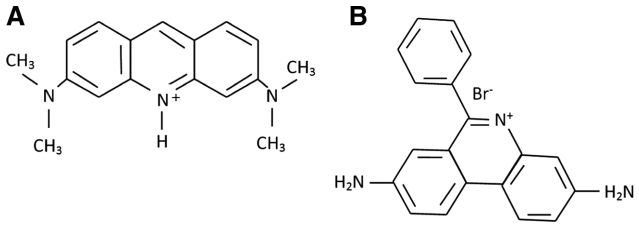

Figure 14 (A) Structure of acridine orange and (B) structure of ethidium bromide.

proton transfer in GC pairs, depurinization, create interstrand crosslinks [27], which are the reason for intercalator ejection from DNA [51]. In its turn, the above influences the efficiency of nonradiative transfer of electronic excitation energy from donor (D) to acceptor (A).

The base of the Förster mechanism of nonradiative transfer of electronic excitation energy is the so-called inductive-resonance transfer of energy from D to A, where dipole-dipole interactions dominates. According to Förster, in our case, the rate of energy transfer k_{ET} is in direct ratio to the donor emission quantum yield (q_{oD}), overlap integral donor emission spectra, and extinction coefficient of acceptor molecule, and inversely to the solvent refraction index in the fourth degree, distance between excited D* and A in the sixth degree, and τ_D is the donor emission decay time [52].

On the other hand, at inductive-resonance transfer of energy through thin dielectric layers with alternative thickness d and permanent concentration of D and A, the following correlation will be achieved [53, 54].

$$\frac{q_D}{q_{oD}}=1-\frac{q_A}{q_{oA}}=\left[1+\left(\frac{d_0}{d}\right)^s\right]^{-1}, \qquad (7)$$

where s=4, 6 and 2 are the energy transfers, consequently, for electric dipole-electric dipole, electric quadruple-electric dipole and magnetic dipole-electric dipole, d_0 is the critical thickness of the layer. Correlation (7) in the case of energy transfer from AO to EB intercalated in the DNA double helix can be rewritten as follows:

$$\frac{q_{AO}}{q_{oAO}}=1-\frac{q_{EB}}{q_{oEB}}=\left[1+\left(\frac{R_0}{R}\right)^s\right]^{-1} \qquad (8)$$

where q_{oD} is the quantum efficiency of donor fluorescence when the distance between energy donor and acceptor $R\to\infty$, q_D at a given R, q_{oA} is the quantum efficiency of sensibilized acceptor fluorescence at $R\to 0$ and q_A at a given R. The value $e_{ET}=1-q_{AO}/q_{oAO}$ was estimated as electron excitation energy transfer efficiency.

So, having a definite concentration of intercalated pair D-A in DNA and changing the concentration of the DNA double helix, the efficiency of energy transfer in the particular D-A pair can be sufficiently changed. Thus, the efficiency of energy transfer is proportional to the DNA double helix site concentration. In Section 3, we show the validity of such an approach for DNA-AO-EB ternary complexes.

Figure 15 shows the fluorescence spectra of binary and ternary AO-DNA and AO-ED-DNA complexes where concentration of DNA changes the distance between donor AO and acceptor EB. AO and EB concentrations were constant and equal to 0.14×10^{-4} mol/l. DNA concentration varied from 0.5×10^{-4} to 10×10^{-4} mol/l per bp. Figure 16 shows the ignition curves of AO fluorescence depending on the distance between AO and EB intercalated in DNA. The distance between donor and acceptor is given in nm and in bp units. The ignition curves of AO fluorescence are built in correspondence to Eq. (8) for the s index equal to 4, 6, or 2. An important characteristic of the energy transfer process is Foerster distance $R_{0.}$. At this distance, half of the donor molecules decay by energy transfer, and the other half decays by the usual radiative and nonradiative rates [55].

$$R_0=0.211\times10^{-1}(k^2n^{-4}q_{oD}J(\lambda))^{1/6}\,(\text{in nm}) \qquad (9)$$

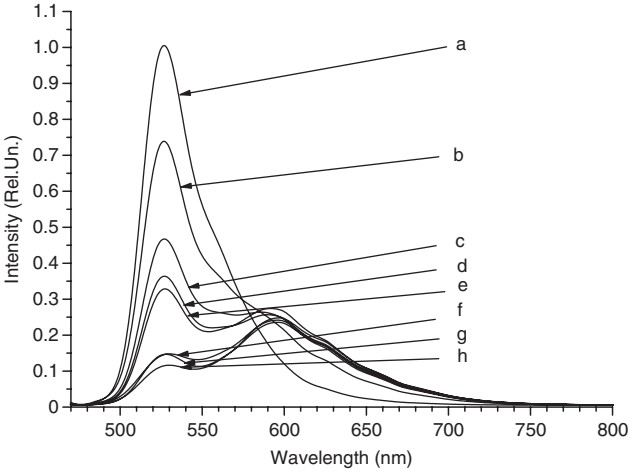

Figure 15 Fluorescence spectra of double and ternary DNA-AO and DNA-AO-EB complexes where concentration of DNA changes the distance between donor AO and acceptor EB. (a) DNA-AO [DNA] – 2.8×10^{-4} mol/l (P), [AO] – 0.14×10^{-4} mol/l, [$NaNO_3$] – 10^{-2} mol/l. (b) DNA-AO-EB [DNA] – 10×10^{-4} mol/l (P), [EB] – 0.14×10^{-4} mol/l, (c) DNA-AO-EB [DNA] – 8×10^{-4} mol/l (P); (d) DNA-AO-EB [DNA] – 6×10^{-4} mol/l (P); (e) DNA-AO-EB [DNA] – 4×10^{-4} mol/l (P); (f) DNA-AO-EB [DNA] – 2.8×10^{-4} mol/l (P); (g) DNA-AO-EB [DNA] – 1.4×10^{-4} mol/l (P); (h) DNA-AO-EB [DNA] – 10^{-4} mol/l (P).

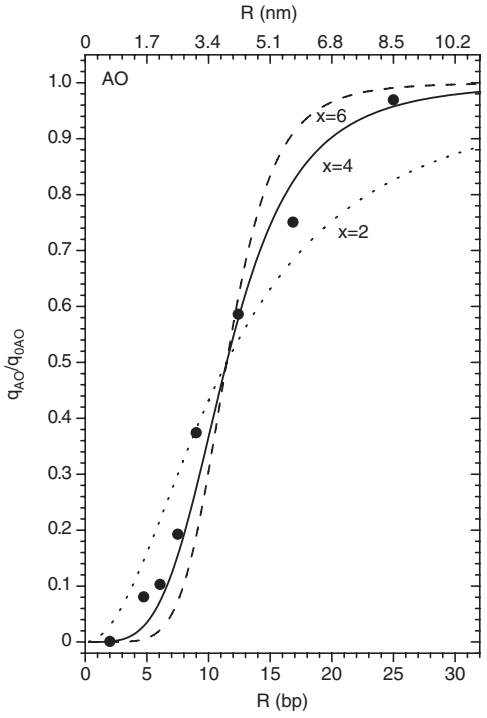

Figure 16 Ignition curves of AO fluorescence depending on the distance between AO and EB intercalated in DNA.

This expression allows to calculate the Förster distance from the spectral properties ($J(\lambda)$) of the donor and the acceptor and the donor quantum yield (q_{0D}), i.e., in terms of the experimentally known values taking into account the environment refractive index (n) and orientation factor (κ^2) of fluorescent molecules. In our case, $J(\lambda)=2.72\times10^{14}$ $(mol/l)^{-1}$ $(cm)^{-1}$ $(nm)^4$, $q_{0D}=0.75$ [56], $\kappa^2=2/3$. For the index of refraction, we choose $n=1.6$ [57]. Thus, the Förster distance is calculated as $R_0=3.5\pm0.3$ nm, which is in good agreement with the experimental value $R_0=3.9\pm0.3$ nm.

Table 3 presents the calculated values for R_0 for different n and κ^2. As a refraction index, some authors use $n=1.33$ (water) [58], others assumed n to be 1.40, which is valid for biomolecules in aqueous solution [55] or $n=1.60$ in the case of DNA [57]. In all cases, any dispersion effects are ignored. The term κ^2 is a factor describing the relative orientation of donor and acceptor transition dipoles in space. κ^2 is usually assumed to be equal to 2/3, which is appropriate for dynamic random average orientation of the donor and acceptor. When donor and acceptor are oriented in parallel planes, then $\kappa^2=1/2$ (for details, see [55]). Evidently, the orientation factor κ^2 and refractive index n for different media do not affect significantly the R_0 value. In Figure 16, we can see that the theoretical curve describing electron excitation transfer for the case electric dipole-electric dipole (S=4) corresponds to experimental data, which is the best. Table 4 gives the values for efficiency $e_{ET}=(1-q_D/q_{OD})$ for AO intercalated in DNA depending on the distance between AO and EB given in bp units. The same table allows to estimate the distance between donor and acceptor in correspondence with the values of e_{ET} evaluated from fluorescence spectra of FRET.

It is well known and it was shown in our work [27] that transition metal ions at the interaction with DNA cause or participate in different conformational changes, e.g., Cu(II) ions initiate DNA transition from B to C form [59]; with the help of TM ions and ethanol, B-Z transition can be initiated [27]. The effect of Ag(I) ions on the DNA structure is known [41]. As early as 1996, we discovered the ejection of AO and EB intercalators from DNA. Besides, the rise in temperature in the solution causes melting of the DNA double helix. In this connection, it was interesting to investigate the electron excitation transfer in D-A pairs intercalated in DNA under the effect of different stress factors with the aim of finding intact sites of DNA double helix.

Table 3 Calculated values of R_0 for different n and k^2.

N	R_0 (bp)		R_0 (nm)	
	$\kappa^2=\frac{2}{3}$	$\kappa^2=\frac{1}{2}$	$\kappa^2=\frac{2}{3}$	$\kappa^2=\frac{2}{3}$
1.33	11.72	11.17	3.98	3.79
1.40	11.32	10.79	3.85	3.67
1.60	10.36	9.87	3.52	3.35

Table 4 Efficiency of energy transfer $e_{ET}=(1-q_D/q_{0D})$ from AO donor to EB acceptor depending on the distance R between them.

e_{ET}	R (bp)	e_{ET}	R (bp)
0.999	1	0.164	16
0.995	2	0.135	17
0.985	3	0.112	18
0.963	4	0.093	19
0.927	5	0.078	20
0.872	6	0.066	21
0.800	7	0.055	22
0.715	8	0.047	23
0.622	9	0.040	24
0.529	10	0.035	25
0.442	11	0.030	26
0.365	12	0.026	27
0.300	13	0.023	28
0.245	14	0.020	29
0.201	15	0.018	30

5 Nanoscale donor-acceptor fluorescent probing of the DNA double helix and stress factors: models and mechanisms

The paragraph is devoted to the effects of Cu(II), Cu(I), and Ag(I) ions, silver nanoparticles, temperature, and laser irradiation on electron excitation energy transfer, efficiency between intercalated in DNA fluorescence molecules of acridine orange (donor) and ethidium bromide (acceptor). Besides, the paragraph deals with the models and mechanisms of DNA defect formation.

Figures 17–20 demonstrate the influence of Cu(II), Cu(I), Ag(I), AgNPs, and laser irradiation (λ=457 nm) on electron excitation energy transfer efficiency from AO to EB intercalated in DNA, which is shown in the rise of effectiveness of FRET. The estimated data are given in Table 4. There are also the data for the distance between AO and EB in bp units, as well as the relative concentrations of DNA sites applicable for intercalation. Figure 17–20 also show that these ions quench AO fluorescence – the phenomena was studied by our group in [36, 51], and it is connected with both dynamic quenching and the quenching caused by nonradiative transfer of excitation energy. On the one hand, Cu(II), Cu(I), Ag(I), AgNPs, and laser irradiation (λ=457 nm) quench AO fluorescence and, on the other hand, increase FRET intensity. It obviously points out that there are different reasons for the phenomenon, in particular, FRET intensity is connected with the quality of double helix, i.e., stability constant of AO and EB with DNA.

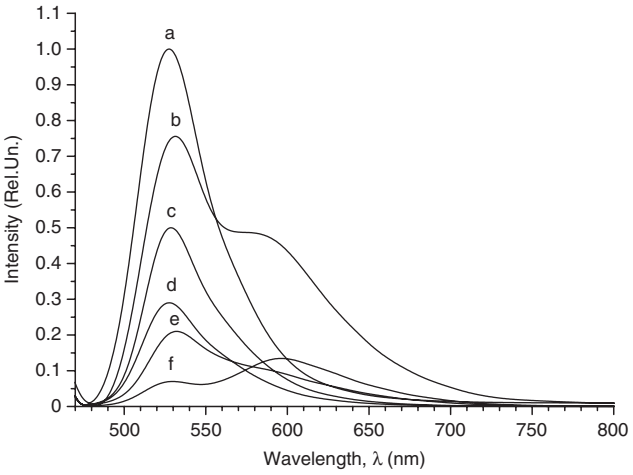

Figure 18 Influence of Cu(I) ([ascorbic acid]/[Cu^{2+}] 2:1) and laser irradiation (λ=457 nm) on electron excitation energy transfer effectiveness from AO to EB intercalated in DNA. (a) DNA-AO; (b) DNA-AO-EB; (c) DNA-AO-Cu(I); (d) DNA-AO-Cu(I) 10-min irradiation; (e) DNA-AO-Cu(I)-EB; (f) DNA-AO-Cu(II) 10-min irradiation+EB. [DNA] – 9.6×10^{-4} mol/l (P), [AO] – 0.14×10^{-4} mol/l, [EB] – 0.14×10^{-4} mol/l, [$CuCl_2$] – 0.14×10^{-4} mol/l, [AA] – 0.24×10^{-4} mol/l, [$NaNO_3$] – 10^{-2} mol/l.

Besides, the temperature effect on FRET stability was investigated. Figure 21 shows the heating effect on DNA solution located in a hermetic test tube in a thermostat. Two milliliters of DNA solution was heated at various temperatures T=323, 333, 343, 353, and 363 K, and then, it was

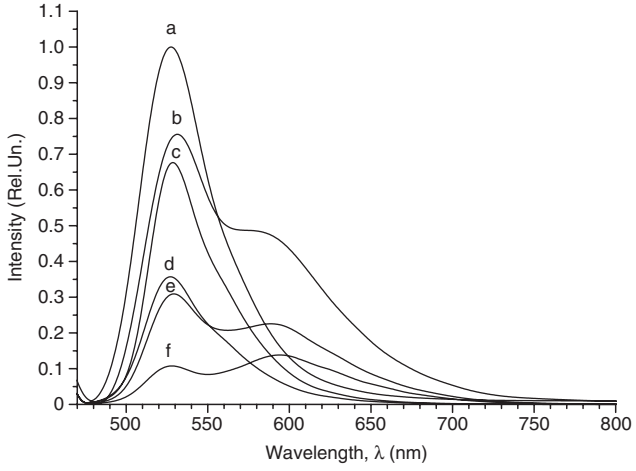

Figure 17 Influence of Cu(II) and laser irradiation (λ=457 nm) on electron excitation energy transfer effectiveness from AO to EB intercalated in DNA. (a) DNA-AO; (b) DNA-AO-EB; (c) DNA-AO-Cu(II); (d) DNA-AO-Cu(II) 10 min irradiation; (e) DNA-AO-Cu(II)-EB; (f) DNA-AO-Cu(II) 10-min irradiation+EB. [DNA] – 9.6×10^{-4} mol/l (P), [AO] – 0.14×10^{-4} mol/l, [EB] – 0.14×10^{-4} mol/l, [$CuCl_2$] – 0.14×10^{-4} mol/l, [$NaNO_3$] – 10^{-2} mol/l.

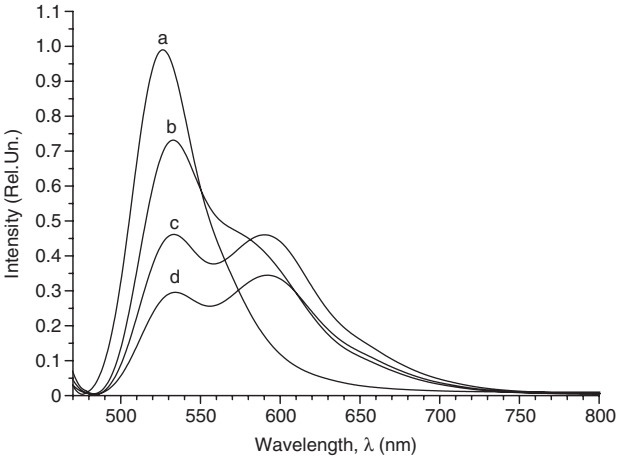

Figure 19 Quenching of fluorescence by Ag^+ ion in DNA-AO-EB complex. (a) DNA-AO, (b) DNA-AO-EB-Ag^+ (C_1), (c) DNA-AO-EB-Ag^+ (C_2), (d) DNA-AO-EB-Ag^+ (C_3). [DNA] – 2.8×10^{-4} mol/l (P), [AO] – $0.14\cdot10^{-4}$ mol/l, [EB] – 0.14×10^{-4} mol/l, [Ag^+] – 0 (C_1), [Ag^+] – 6.0×10^{-6} mol/l (C_2), [Ag^+] – 30.0×10^{-6} mol/l (C_3), [$NaNO_3$] – 10^{-2} mol/l. λ=460 nm.

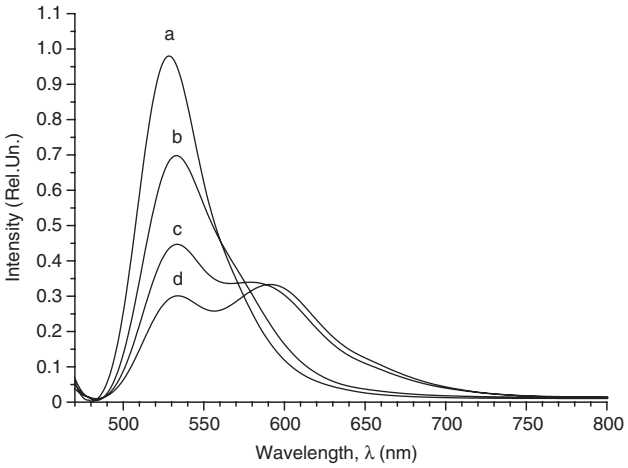

Figure 20 Quenching of fluorescence by AgNPs in DNA-AO-EB complex. (a) DNA-AO, (b) DNA-AO-EB-AgNPs (C_1), (c) DNA-AO-EB-AgNPs (C_2), (d) DNA-AO-EB-AgNPs (C_3). [DNA] – 2.8×10^{-4} mol/l (P), [AO] – 0.14×10^{-4} mol/l, [EB] – 0.14×10^{-4} mol/l, [AgNPs] – 0 (C_1), [AgNPs] – 6.0×10^{-6} mol/l (C_2), [AgNPs] – 18.0×10^{-6} mol/l (C_3), [$NaNO_3$] – 10^{-2} mol/l. λ=460 nm.

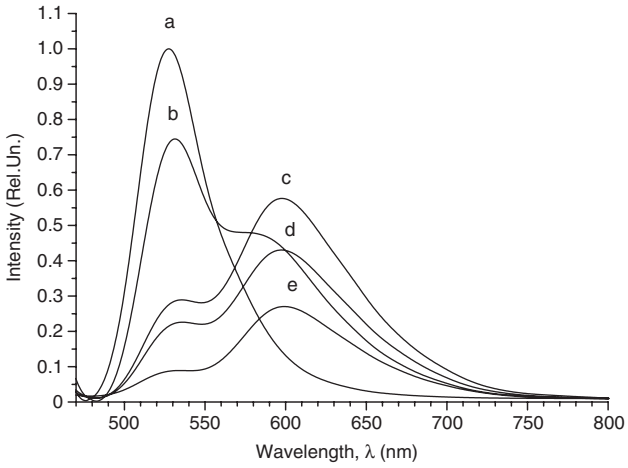

Figure 22 Fluorescence spectra for ternary complexes AO-DNA-EB. The complexes were prepared as follows: DNA solutions put in hermetic test tubes were kept *in vitro* in thermal bath at a temperature of 100°C for different periods of time (5, 10, and 20 min). (a) DNA-AO, (b) DNA-AO-EB (0 min), (c) DNA-AO-EB (5 min), (d) DNA-AO-EB (10 min), (e) DNA-AO-EB (20 min). [DNA] – 2.8×10^{-4} mol/l (P), [AO] – 0.14×10^{-4} mol/l, [EB] – 0.14×10^{-4} mol/l, [$NaNO_3$] – 10^{-2} mol/l.

taken out and put into an icy bath (T=273 K). At 293 K, an intercalator pair AO-EB was added to the solution, and the fluorescence spectra were registered.

Figure 22 shows the fluorescence spectra for ternary complexes AO-DNA-EB. The complexes were prepared as follows: DNA solutions put in hermetic test tubes were kept *in vitro* in thermal bath at the temperature 373 K for different periods of time (5, 10, and 20 min). Then, they were quickly cooled in an icy bath (T=273 K). After the procedure, the intercalator pair AO-EB was added to the solution, and fluorescence spectra were registered. From the spectra given in Figures 21 and 22, and with the application of Table 4, the effectiveness of FRET, the data for the distance between AO and EB in bp units, as well as the relative concentrations of DNA sites applicable for intercalation were estimated. The results are given in Table 5.

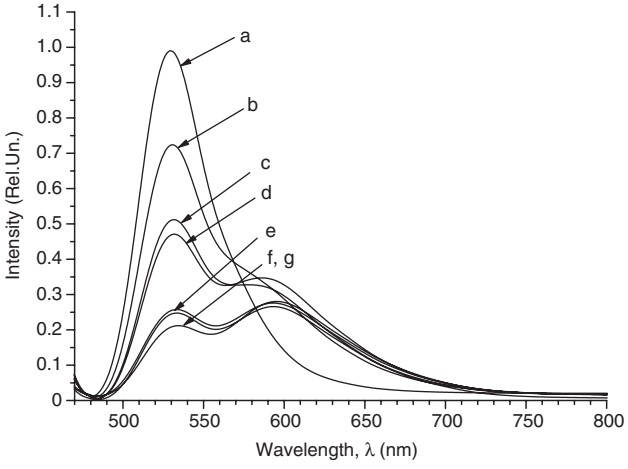

Figure 21 Heating effect on DNA solution located in a hermetic test tube in thermostat at various temperatures t=323, 333, 343, 353 and 363K. (a) DNA-AO, (b) DNA-AO-EB, (c) DNA-AO-EB 323K, (d) DNA-AO-EB 333K, (e) DNA-AO-EB 343K, (f) DNA-AO-EB 353K, (g) DNA-AO-EB 363K . [DNA] – 2.8×10^{-4} mol/l (P), [AO] – 0.14×10^{-4} mol/l, [EB] – 0.14×10^{-4} mol/l, [$NaNO_3$] – 10^{-2} mol/l.

Figure 23 presents changes in the values of the AO molecule (λ=502 nm) absorption spectra maximums in water solutions and in binary and ternary complexes with DNA-AO and DNA-AO-Cu(II), Cu(I), and Ag(I). Analyzing the data, we can see that Cu (II) and Cu (I) ions decrease the destructive effect of irradiation, while Ag(I) ions increase it.

Figure 24 shows the change of energy transfer efficiency from 13 bp to 7 bp from AO to ethidium bromide intercalated in DNA after 20 min of irradiation of the binary DNA-AO complex (see Table 5).

The following paragraphs will show new models and mechanisms of defect formation in DNA caused by stress factors.

5.1 Double proton transfer in GC pairs in DNA

The influence of H^+ ions on UV spectra of guanine and cytosine has been known for a long time [60, 61] as well as its

Table 5 Cu(II), Cu(I), Ag(I) ions, AgNP, laser irradiation (λ=457 nm), and heating effects on e_{ET}[a] and $C^{st}_{dh}/C_0 = R^{st}_{AO\text{-}EB}/R^{0}_{AO\text{-}EB}$[b].

Stress factor for DNA-AO-EB[c]	e_{ET} (%)	$R_{AO\text{-}EB}$ (bp)[d]	$\frac{C^{st}_{dh}}{C_0} = \frac{R^{st}_{AO\text{-}EB}}{R^{0}_{AO\text{-}EB}}$
–	20	15	1
Cu(II)	58	10–9	0.63
Cu(I)	53	10	0.67
Ag(I)	67	8–9	0.57
AgNPs (1)	62	9	0.6
AgNPs (2)	76	8–7	0.5
Heating			
20°C	20	15	1
50°C	48	10–11	0.7
60°C	52	10	0.67
70°C	76	8–7	0.5
80°C	81	7	0.47
90°C	82	7	0.47
Boiling			
20°C	30	13	1
100°C, 5 min	80	7	0.54
100°C, 10 min	87	6	0.46
100°C, 20 min	95	4	0.31
Laser irradiation			
DNA-AO 25 min	30	13	0.54
Cu(II) (10 min)	77	8–7	0.5
Cu(I) (10 min)	81	7	0.47

[a]Foerster resonance electron excitation energy transfer from donor AO to acceptor EB. [b]Relative concentration of DNA double helix areas applicable for AO and EB intercalation, where C^{st}_{dh} is the concentration of double helix areas in bp left after stress effect, C_0 is the initial DNA concentration in mol/l bp, $R^{0}_{AO\text{-}EB}$ is the distance between AO and EB at initial DNA concentrations, $R^{st}_{AO\text{-}EB}$ is the distance between AO and EB after stress; [c]different effects on DNA double helix; [d]$R_{AO\text{-}EB}$ is the distance between AO and EB in bp units evaluated from efficiency e_{ET} (see Table 4).

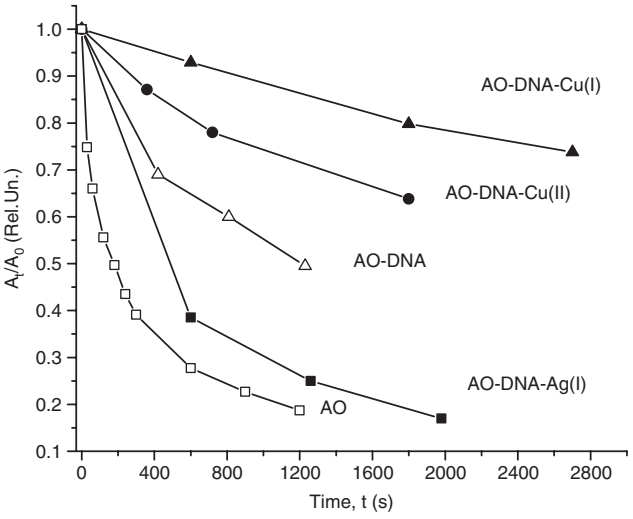

Figure 23 Laser irradiation effect on AO molecules in binary and ternary complexes AO-DNA, AO-DNA-Cu(II), AO-DNA-Cu(I), DNA-AO-Ag, and AO. ▸—AO-DNA-Cu(I); •—AO-DNA-Cu(II), △—AO-DNA, ■—DNA-AO-Ag(I) □—AO. [DNA] – 0.7×10^{-3} mol/l (P), [AO] – 0.7×10^{-4} mol/l, [EB] – $0.7\cdot10^{-4}$ mol/l, [AA] – 1.4×10^{-4} mol/l, [Ag^+] – 0.7×10^{-4} mol/l, [$CuCl_2$] – 0.7×10^{-4} mol/l, [$NaNO_3$] – 10^{-2} mol/l.

explanation by keto-enolic and amino-imino transformations in guanine and cytosine, correspondingly. It should be noted that the mentioned transfers of proton ions between proton-donor and proton-acceptor groups N1 and O6 in guanine and N4 and N3 in cytosine are definitely performed with the help of the hydrated H_2O molecules; they form a kind of cyclic structures with the above groups in guanine and cytosine. Because of the self-congruent transition of protons from N1 of guanine and N4 of cytosine to a molecule of hydrated H_2O, reorientation of H_2O molecules takes place in both cases.

Thus, we can state that the specific energy of H bonds with two energy states and self-congruent transfer of protons in cyclic structures is a necessary and sufficient condition for keto-enol and amino-imino tautomeric transformations of polar organic molecules, particularly guanine, cytosine, and adenine in solution. Water molecules act as a mediator in the process of forming the joint electron-proton complementary complex between the proton-acceptor/donor groups of the solute molecules and those of the solvent. So, here there is no need for water molecules as mediators in the DNA duplex because a pair of complementary bases always forms a cyclic structure.

Double proton transfer (DPT) in DNA is demonstrated spectroscopically as bathochromic shifts, weak

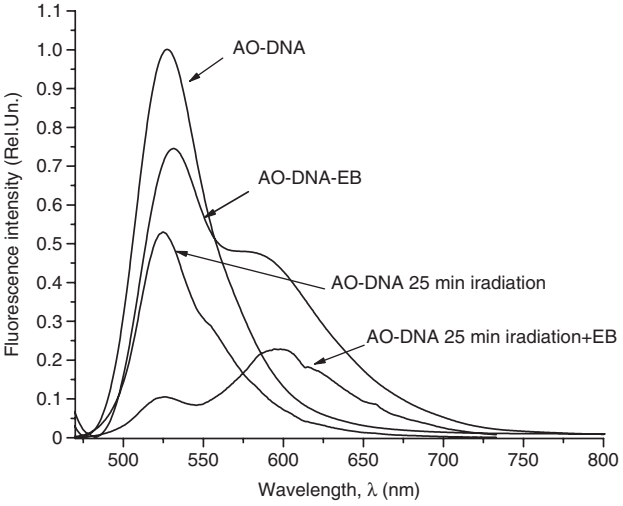

Figure 24 Influence of laser irradiation (λ=457 nm) on electron excitation energy transfer effectiveness from AO to EB intercalated in DNA. (A) AO-DNA; (B) AO-DNA-EB; (C) AO-DNA irradiation 25 min; (D) AO-DNA irradiation 25 min+EB. [DNA] – 7×10^{-4} mol/l (P), [AO] – 0.14×10^{-4} mol/l, [EB] – 0.14×10^{-4} mol/l, [$NaNO_3$] – 10^{-2} mol/l.

hypochromic effects, and small widening of the absorption band [27, 36]. We shall discuss the mechanism in detail, using GC pairs as an example for the following reasons:

1. the effect of H^+ interactions with guanine and cytosine [41, 62], as well as the interaction between transition metal ions and guanine are easily observed in the UV spectra;
2. spontaneous mutations of a genome occur more often at GC pairs than at AT pairs [63–65];
3. guanine and cytosine are often populated with rare enol and imino forms [66–68];
4. GC pairs are far less resistant to tunneling transitions compared to AT pairs [69–71];
5. in the DNA duplex, the site of preferable binding of H^+ and metal ions is the endocyclic N7 of guanine located in the major groove [31, 32].

In general, the keto-enol and amino-imine tautomeric transformations in GC pairs are conditioned by the electric charges on G-N1 and C-N3 of endocyclic nitrogens, which play the principal role in H bonding of the base pairs. Figure 25 illustrates double-proton transfer in GC pair of DNA.

5.2 Interstrand crosslinks in the DNA double helix: ion sorption as a multistage adsorption process

Soft ions, in particular, Cu(I), Ag(I), Pt(II), Hg(II) ions are able to form the so-called interstrand crosslinks in DNA [60]. Let us consider the process on the example of Ag(I). First, silver ions are adsorbed on the DNA major groove (Guanine-N7 (G-N7) or chelate complex G-N7 and G-O6). At small silver ion concentration on DNA does not cause ejection of AO and EB [36]. On the other hand, silver ions at an interaction with DNA induce double proton transfer in the GC pair (see Section 5.1). Chelate complex with silver ions makes it easy to unfold the DNA double helix with the wrong Watson-Crick GC pair. In this process, guanine's atom O6 is in the enol form, the nitrogen atom G-N1 is in the pyridine state and cytosine-N3 (C-N3) is in the pyrole state. After unfolding of the double helix in neutral water solution the C-N3 atom cannot keep the enol state for a long time, and it should transfer into its usual pyridine state. At the same time, silver ions can, with definite possibility, attack nitrogen atoms G-N1 still existing in the pyridine state. During the following folding of the double helix, inter-crosslink formation between G*-N1 and C-N3 takes place. In this way, the process of inter-crosslink formation can be considered as such a simple process as 1. Silver ion adsorption on DNA (G-N7) and double proton transfer of GC pair with the lifetime τ_1, 2. The unfolding of the double helix causes the formation of G*-N1- Ag^+ binding, C-HN3 transfer to C-N3 and formation of link between G*-N_1-Ag+-C-N_3. The total time of the process is τ_2, 3. DNA folding with the formation of a stereoscopically distorted double helix with inter-crosslinks (τ_3). So, in the case of the DNA compound, the absorption process of inter-crosslink formation can be reduced to a multistage adsorption process consisting of several simple adsorption processes named above with the total time of $\tau_1+\tau_2+\tau_3$. Scheme 1 illustrates it.

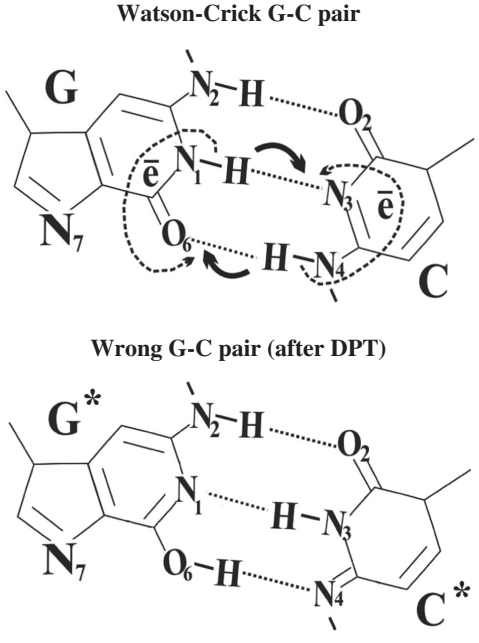

Figure 25 Double proton transfer (DPT) in a G-C part of DNA.

5.3 Glycoside linkage [C(I)-N(9)] hydrolysis in DNA – depurinization

Depurination: Interaction of H^+ and Me^{n+} with N(3) and N(7) of guanine in DNA with certain probability leads

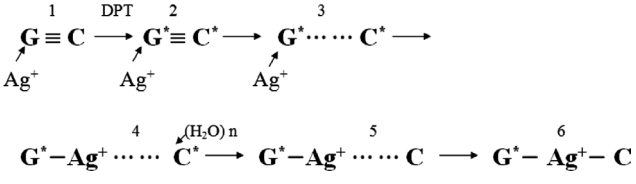

Scheme 1 The interstrand crosslink in DNA induced by silver ions. 1. Regular Watson-Crick pair. 2. Wrong Watson-Crick pair. 3. Open pair. 4. In the open wrong pair, silver ions start to transfer from N7 to N1. 5. In the open pair, the cyclic water molecules system makes proton transfer from N3 to N4 in cytosine. 6. The interstrand crosslink.

to DPT, on the one hand, and to hydrolysis of glycosidic linkage C(1)-N(9), on the other.

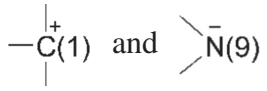

The reaction takes place with the participation of dissociated molecules of H_2O (OH^- and H^+). Of course, H^+ approaches the negatively charged N^- as OH^- goes to C^+:

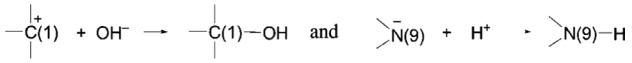

It needs to be mentioned that depurination can take place only in unwinded sites of the DNA double helix. The dependence of the probability of unwinding of the central AU and GC base pairs in RNA double helix on the adjacent pairs was investigated in [22], and it was shown that the probability of opening of the G-C pair is minimum and equal to 0.3×10^{-5} in sequence:

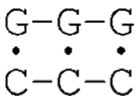

and the probability of opening of the A-U is maximum and equal to 120×10^{-5} in sequence:

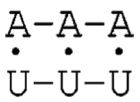

5.4 Phosphordiester linkage hydrolysis in DNA: photodynamic effect and the Jablonski diagram

The hydrolysis reaction requires the presence of H^+ and OH^- ions, the concentration of which in water at pH=7 (natural pH for living cell) is 10^{-7}mol/l, i.e., the electric dissociation constant is 10^{-14}. Naturally, at such concentrations, the probability to hydrolysis is very small. *In vivo* phosphordiester link hydrolysis in DNA and RNA is carried out by nuclease ferments (DNase and RNase), and *in vitro* photoenergy dissipation in solution acts as a catalyst, first of all, in phosphordiester and glycoside link hydrolysis reactions in Figure 26. It cannot be excluded that in discoloration and degradation of aromatic compounds, the hydrolysis reaction is also important. A lifetime (τ) of exited AO singlet state is ~10^{-9} s ($\tau_{AO}=1.5\times10^{-9}$, $\tau_{AO\text{-}DNA}=5.2\times10^{-9}$ s [72]), the possibility that the oxygen molecule ($[O_2]=1.3\times10^{-6}$ mol/l at T=298 K, see Table 2) can collide with the AO molecule is too small. At the same time, the triplet excited state is unusual for AO molecule at room temperature [73, 74].

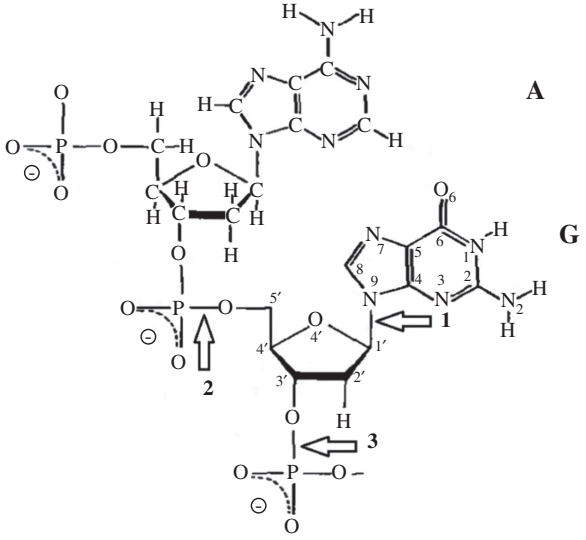

Figure 26 Segment of polynucleotide DNA change 1- glycoside link, 2- and 3- phosphordiester links.

So, in the case of the DNA complex with AO at photodynamic effect in solutions, the principal oxidant is not an oxygen molecule but H^+ ions. It is also connected to the fact, which we have shown, that for H^+ ions, the mobile adsorption state of DNA is typical. It should be noted that at the photodynamic effect, the H^+ local concentration depends on electrolytic dissociation of the water molecule. So, at photon absorption by chromophore, a part of energy dissipates into heat as a result of conversion, which we consider as energy transfer from electron vibration levels of organic molecules (in our case AO) to water molecule vibration levels (see IRET in Figure 27), and it should increase the constant of electrolytic dissociation. For instance, a 373 K temperature rise causes increase in water dissociation constant by three orders (Arrhenius equation). It is interesting how many H^+ and OH^- ions one photon (λ=457 nm) can generate if it totally dissipates into heat. As electrolytic dissociation reaction activation energy requires 81.6 kJ/mol, the energy of the absorbed photon is enough for three water molecules to undergo electrolytic dissociation. In the place where the AO exited molecule undergoes total energy dissipation, we can get high local concentration of H^+ and OH^- ions in immediate proximity from DNA and, thus, the possibility to hydrolysis both phosphordiester and glycoside is significant. In particular, phosphor-di-ester links a) $P\text{-}O_{(3')}$ and b) $O_{(5')}\text{-}P$ can be presented as two schemes.

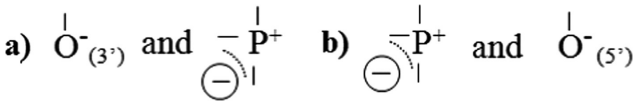

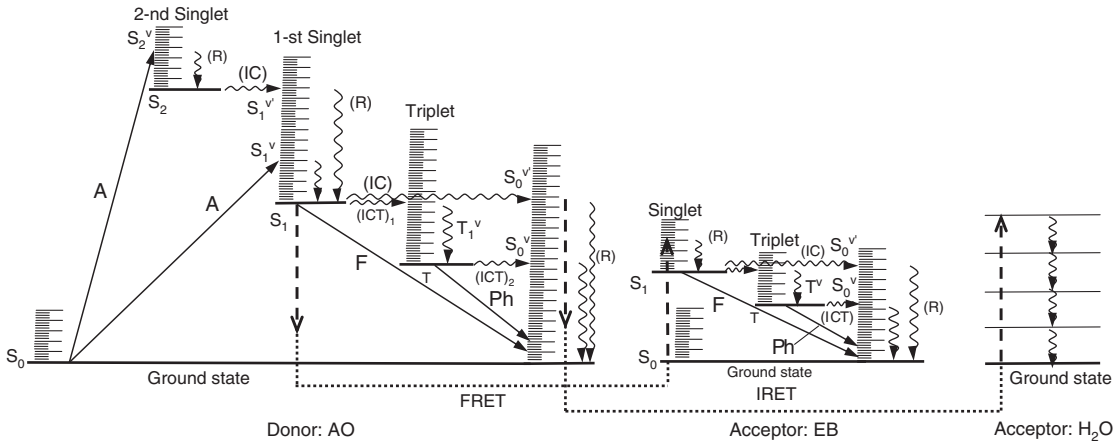

Designation	Photophysical process	Rate, s^{-1}
A	Photon absorption: instantaneous process	-
F	Fluorescence: singlet-singlet photon emission	~10^9
Ph	Phosphorescence: triplet-singlet photon emission	10^{-2}-10^3
ICT	Intercombination transition: nonradiative spin inversion (S→T or T→S change ofmultiplicity)	$<10^{-1}$-10^2
IC	Internal conversion:nonradiative (thermal) relaxation of molecule to the electron level of same multiplicity (e.g. $S_2 \rightarrow S_1$)	10^{11}
R	Rovibron relaxation from excited vibroniclevel to the zero level of the same (as usual) state (e.g. $S_1^{v4} \rightarrow S_1^{v0}$)	10^{12}-10^{14}
FRET	Fluorescence resonance energy transfer	10^{12}-10^{13}
IRET	Inductive resonance energy transfer from excited intercalator to water molecules with resonance overtone vibration of OH.	10^{12}-10^{14}

Figure 27 Scheme of electron-vibration-rotation levels of intramolecule transitions in compound organic molecules and singlet-singlet energy transfer between donor and acceptor.

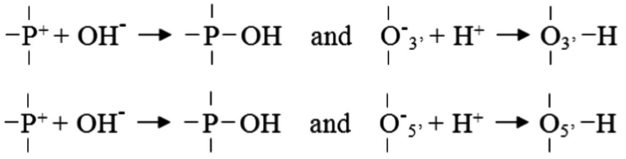

6 Conclusions

Using spectrophotometry and thermodynamic approaches, we have shown that 1) on interaction with DNA, silver nanoparticles with the size 1–2 nm (AgNPs) are adsorbed, and only partial corrosion of nanoparticles at the level of Ag^+ ions is observed; 2) AA reduces silver ions in ternary complex DNA-$AgNO_3$-AgNPs. Thus, AgNPs activate the process of quick reduction of Ag^+ ions to silver atoms; 3) at photo-irradiation (λ=436 nm or full spectrum of visible band) desorption of silver atoms from the surface of AgNPs takes place. The atoms are first adsorbed on the surface of DNA and then penetrate inside the double helix (crosslinks between complementary DNA base pairs) making a prolate stretched structure (AgNPs absorption spectrum width is changed from 140 nm to 360 nm at half-height); 4) the kinetic study of photodesorption makes it possible to determine the desorption rate constant k_d and adsorption heat Q_a that are equal to $k_d \cong 9\times10^{-5}$ s^{-1}; $Q_a \geq 80$ kJ/mol Ag^0 for AgNPs bound with DNA; 5) AgNPs represent liquid drops, which moisturize the DNA surface at interaction. At photo-irradiation of the AgNPs-DNA complex, DNA-dependent conformational transition takes place due to fast and intensive heating.

The nano-scale method of laser-induced fluorescence resonance energy transfer (FRET) to donor-acceptor intercalator pair for quantitative and qualitative study of stability quality, the DNA double helix in solution in real time is offered. The approach is based on the example of the acridine orange molecule (donor) and ethidium bromide (acceptor) intercalated in DNA.

It is shown that ions Cu(II), Cu(I), Ag(I), and AgNPs, laser irradiation of AO, and the effect of heating decrease the concentration of undamaged areas of DNA double helix, i.e., the sites able to intercalate dye molecules such as AO and EB.

FRET radii were experimentally estimated in the background electrolyte solution (0.01 mol/l $NaNO_3$) and proved to be 3.9±0.3 nm, and the data are in satisfactory agreement with the theoretically calculated value R_0=3.5±0.3 nm.

The FRET method allows to estimate the concentration of double helix areas with high quality stability applicable for intercalation in DNA after it was subjected to a stress effect. It gives the opportunity to compare various

types of DNAs with 1) different origins; 2) various damage degrees; 3) and in various functional states.

Alternative models and mechanisms of photodynamic effect on DNA in solutions are proposed. They are based on photo energy degradation in solutions. The energy activates electrolytic dissociation of water molecules on H_3O^+ and OH^- and acts as a catalyst for hydrolysis reactions of phosphor-di-ester and glycoside linkages.

7 Experimental part

7.1 Materials

7.1.1 DNA

In our tests, we used the calf thymus DNA (40% GC), Sigma-Aldrich (GPC JSC Tbilisi, Georgia). The concentration of nucleic acids was determined by UV absorption using molar extinction coefficients (ε=6600 cm/(mol/l) at λ=260 nm). The double helix structure of the polymers was proved by their hyperchromicity (>30%) and their typical thermal denaturation transition (measured in 0.01 mol/l $NaNO_3$, pH≅6.0). pH was checked by a pH meter HANNA Instruments pH213 (Woonsocket, USA).

7.1.2 Intercalators

Acridine orange (AO) was purchased from Sigma-Aldrich (GPC JSC Tbilisi, Georgia). The concentration of the dye was determined colorimetrically at the isobestic point of the monomer-dimer system (λ=470 nm) using the molar extinction coefficients (ε=43 300 cm/(mol/l)). Ethidium bromide (EB) was also purchased from Sigma-Aldrich (GPC JSC Tbilisi, Georgia). The concentration of the dye was determined colorimetrically (ε=5600 cm/(mol/l) at λ=480 nm).

7.1.3 Ions

We used chemically pure copper chloride. Bidistillate water served as a solvent. In tests with Ag(I) ions, chemically pure salts $AgNO_3$ were used, and $NaNO_3$ served as background electrolytes. All chemicals were purchased from Sigma-Aldrich, GPC JSC Tbilisi, Georgia.

7.1.4 Nanoparticles

Colloidal silver suspension with particle sizes of 1–2 nm in distilled water (200 μg/ml) was purchased from DDS Inc (D/B/A, Amino Acid & Botanical Supply, Cedar Knolls, NJ, USA).

7.2 Instrumentation

7.2.1 Absorption spectra

Absorption spectra of DNA complexes with intercalators AO and EB were registered in real time using charge-coupled device (CCD) spectrometer AvaSpec ULS 2048-USB2. It should be underlined that registration of fluorescence spectra excited by laser irradiation is necessary to carry out in real time as, at such, excitation of intercalators, AO in particular, its fast photo-oxidation takes place.

7.2.2 Diode laser

Diode laser SDL-475-100T (Shanghai Dream Lasers Technology Co., Ltd., Shanghai, China) was used for irradiation and excitation (λ=457 nm with optical beam cross section 2 mm, and P=200 mW) of laser-induced fluorescence spectra.

7.2.3 Photoirradiation

Photoirradiation was carried out in a reactor with the fixed light beam in 1-cm rectangular fluorescent quartz cell. In the same cell with the interval of 5 min absorption spectra of irradiated solutions were registered by AvaSpec spectrometer (Apeldoorn, The Netherlands). Before each absorption registration, the cell was shut to protect the solution from photo irradiation. Registration time was 8 ms. As a source of radiation, xenon arch discharge lamp with rating of 35 W in glass balloon was used. To irradiate the solution, water filter and light filter with light wave transmission (λ=436 nm were used. Radiation power in the cell was 300 mW for thermal water filter and 15 mW for water filter matched with light filter (λ=436 nm).

Acknowledgments: The authors express their gratitude to Prof. Henri Kagan, Paris-Sud University, Orsay, for his permanent kind attention to our work. They also express gratitude to Prof. Jamlet Monaselidze for usefull discussions, Dr. Jemal Chkhaberidze for some valuable data, and to Mrs. Greta Nijaradze for her help in preparing the original manuscript. The work was partly supported by the grants of Shota Rustaveli National Science Foundation: GNSF/ST09_508_2-230, GNSF41/14, GNSF 12/24, GNSF-STCU #5622. This work is supported by the IPP/ISTC A-1951 Project.

References

[1] Matczyszyn M, Olesiak-Banska J. DNA as scaffolding for nanophotonic structures. *J. Nanophotonics* 2012, 6, 064505.

[2] Garcia-Parajo MF. Optical antennas focus in on biology. *Nat. Photonics* 2008, 2, 201–203.

[3] Chevrier DM, Chatt A, Zhang P. Properties and applications of protein-stabilized fluorescent gold nanoclusters: short review. *J. Nanophotonics* 2012, 6, 064504.

[4] Falanga A, Tarallo R, Galdiero E, Cantisani M, Galdiero M, Galdiero S. Review of a viral peptide nanosystem for intracellular delivery. *J. Nanophotonics* 2013, 7, 071599.

[5] Blum C, Zijlstra N, Lagendijk A, Wubs M, Mosk AP, Subramaniam V, Vos WL. Nanophotonic control of the Förster resonance energy transfer efficiency. *Phys. Rev. Lett.* 2012, 109, 203601.

[6] Huang X, Jain PK, El-Sayed IH, El-Sayed MA. Plasmonic photothermal therapy (PPTT), *Lasers Med. Sci*. 2008, 23, 217–228.

[7] Lopotko D. Therapy with gold nanoparticles and lasers: what really kills the cells? *Nanomedicine* 2009, 4, 253–256.

[8] Pissuwan D, Valenzuela SM, Cortie MB. Therapeutic possibilities of plasmonically heated gold nanoparticles, *Trends Biotechnol.* 2006, 24, 62–67.

[9] Yang K, Zhang S, Zhang G, Sun X, Lee S-T, Liu Z. Graphene in mice: ultrahigh in vivo tumor uptake and efficient photothermal therapy. *Nano Lett.* 2010, 10, 3318–3323.

[10] Chen X, Zehnbauer B, Gnirke A, Kwok PY, Fluorescence energy transfer detection as a homogeneous DNA diagnostic method. *Proc. Nat. Acad. Sci. USA* 1997, 94, 10756–10761.

[11] Sekar RB, Periasamy A. Fluorescence resonance energy transfer (FRET) microscopy imaging of live cell protein localizations. *J. Cell Biol*. 2003, 160, 629–633.

[12] Chang CW, Wu M, Merajver SD, Mycek MA. Physiological fluorescence lifetime imaging microscopy improves Förster resonance energy transfer detection in living cells. *J. Biomed. Opt.* 2009, 14, 060502.

[13] Hovan SC, Howell S, Park PS-H. Förster resonance energy transfer as a tool to study photoreceptor biology. *J. Biomed. Opt.* 2010, 15, 067001.

[14] Wang Y, Wang LV. Förster resonance energy transfer photoacoustic microscopy. *J. Biomed. Opt.* 2010, 17, 086007.

[15] Siegel AP, Hays NM, Day RN. Unraveling transcription factor interactions with heterochromatin protein 1 using fluorescence lifetime imaging microscopy and fluorescence correlation spectroscopy. *J. Biomed. Opt.* 2013, 18, 025002.

[16] Mochizuki K, Kondo T, Nakazawa T, Iwashina M, Kawasaki T, Nakamura N, Yamane T, Murata S, Ito K, Kameyama K, Kobayashi M, Katoth R. RET rearrangements and BRAF mutation in undifferentiated thyroid carcinomas having papillary carcinoma components. *Histopathology* 2010, 57, 444–450.

[17] Feng F, Liu L, Wang S. Fluorescent conjugated polymer-based FRET technique for detection of DNA methylation of cancer cells. *Nat. Protoc.* 2010, 5, 1237–1246.

[18] Lu S, Wang Y. FRET biosensors for cancer detection and evaluation of drug efficacy. *Clin. Cancer. Res*. 2010, 16, 3822–3824.

[19] San Martín A, Ceballo S, Ruminot I, Lerchundi R, Frommer WB, Barros LF. A genetically encoded FRET lactate sensor and its use to detect the Warburg effect in single cancer cells. *PLoS One* 2013, 8, e57712.

[20] Yakushevich LV. DNA dinamics. *Mol. Biol. (Russia)* 1989, 23, 652–662.

[21] Pohl FM, Jovin TM. Salt-induced co-operative conformational change of a synthetic DNA: equilibrium and kinetic studies with poly (dG-dC). *J. Mol. Biol.* 1972, 67, 375–396.

[22] Gralla J, Crothers DM. Free energy of imperfect nucleic acid helices. 3. Small internal loops resulting from mismatches. *J. Mol. Biol.* 1973, 78, 301–319.

[23] Weiner PK, Langridge R, Blaney JM, Shaefler R, Kollman P. *Proc. Natl. Acad. Sci. USA* 1982, 79, 3754.

[24] Lavery R, Pullman B. The molecular electrostatic potential and steric accessibility of poly (dI. dC). Comparison with poly (dG. dC). *Nucleic Acids Res.* 1981, 9, 7041–7052.

[25] Lavery R, Cauchy D, De La Luz Rojas O, Pullman A. Molecular electrostatic potential of the B-DNA helix., VII. Effect of screening by monovalent cations. *Int. J. Quant. Chim. Acta* 1980, 7, 323–330.

[26] Manning GS. The molecular theory of polyelectrolyte solutions with applications to the electrostatic properties of polynucleotides. *Q. Rev. Biophys.* II, 1978, 2, 179–246.

[27] Bregadze V, Gelagutashvili E, Tsakadze K. Thermodynamic models of metal ion-DNA interactions. In *Metal-Complex DNA Interactions*, Hajiliadis N, Sletten E, Eds., Blackwell Publishing: Oxford, UK, 2009, pp. 31–53.

[28] Bell, RP. *The Proton in Chemistry*, Champan and Hall: London, 1973.

[29] Cairns, J. The application of autoradiography to the study of DNA viruses. *Cold Spring Harbor Symp. Quant Biol*. 1962, 27, 311–318.

[30] Chkhaberidze JG. *Metal Ions Effect on Dye Fluorescence and Intercalation in DNA,* Institute of Physics of Georgian AS, PhD Thesis, Tbilisi, 1996.

[31] Saenger W. *Principles of Nucleic Acid Structure*, Springer-Verlag: New York Inc., 1984.

[32] Bregadze VG. Metal ions interactions with DNA: considerations on structure, stability, and effects from metal ions binding. In *Metal Ions in Biological Systems*, Vol. 32, Chap. 12, Sigel A, Sigel H, Eds., Marcel Dekker: New York, 1996, pp. 419–451.

[33] Frenkel J. Theorie der adsorbtion und verwandter erscheinungen. *Z.Phys* 1924, 26, 117.

[34] Frenkel J. *Statistical Physics*, Acad. Sci. USSR: Moscow – Leningrad, 1948.

[35] Slutsker AI, Mikhailin AL, Slutsker IA. Microscopics of energy fluctuations of atoms in solids. *Physics-Uspekhi (Nauk)* 1994, 164, 357–366.

[36] Bregadze VG, Khutsishvili IG, Chkhaberidze, JG, Sologashvili, K. DNA as a mediator for proton, electron and energy transfer induced by metal ions. *Inorganica Chim. Acta* 2002, 339, 145–159.

[37] Bregadze VG, Melikishvili ZG, Giorgadze TG. Photo-induced DNA-dependent conformational changes in silver nanoparticles. *Adv. Nanopart.* 2013, 2, 176–181.

[38] Bregadze VG. Nature of DNA interactions with cations: UV spectroscopic investigation and Marcus theory. *Int. J. Quantum Chem*. 1980, XVII, 1213–1219.

[39] Hart EJ, Anbar M. The hydrated electron, *Atomizdat*, *Moscow*, 1973, p. 280.

[40] Bregadze VG. Metal ion interactions with DNA: consideration on structure, stability, and effects from metal ion binding. In *Metal Ions in Biological Systems*, Sigel A, Sigel H, Eds., Marcel Dekker: New York, 1996, 32, pp. 453–474.

[41] Wilhelm FX, Daune M. Interactions des ions métalliques avec le DNA. III. Stabilité et configuration des complexes Ag-DNA. *Biopolymers* 1969, 8, 121–137.
[42] Davidov AS. *Theory of Molecular Excitons*, McGrow-Hill Book Company: New York, 1962.
[43] Tinoco J, Halpern A, Simpson W. The relation between conformation and light absorption in polypeptides and proteins. In *Polyamino Acids, Polypeptides and Proteins*, Univ. Wesconsin Press: Madison, Wisconsin, 1962, 147–160.
[44] The Effect of Size on Optical Properties: Data of Firm NanoComposix, Silver Nanoparticles: Optical Properties. http://nanocomposix.com/kb/silver/optical-properties.
[45] Yanari S, Bovey FA. Interpretation of ultraviolet spectral changes of proteins. *J. Biol. Chem*. 1960, 235, 2818–2826.
[46] Nir S, Abams S, Rein R. Polarizability calculations on water, hydrogen, oxygen, and carbon dioxide. *J. Chem. Phys*. 1973, 59, 3341–3355.
[47] The Effect of Aggregation on Optical Properties: Data of Firm NanoComposix, Silver Nanoparticles: Optical Proper-ties. http://nanocomposix.com/kb/silver/optical-properties.
[48] Volkenshtein MV. *Molecular Biophysics*, Nauka: Moscow, 1975.
[49] Higasi K, Baba H, Rembaum A. *Quantum Organic Chemistry*, Nterscience Publishers: New York, 1965.
[50] Chemical Encyclopaedia (in Russian), "Clusters," Vol. 2, *Sovetskaia Entsiklopedia*, Moscow, 1990.
[51] Bregadze VG, Chkhaberidze JG, Khutsishvili IG. Effect of metal ions on the fluorescence of dyes bound to DNA. In *Metal Ions in Biological Systems*, vol. 33 (chapter 8), Sigel A, Sigel H, Eds., Marcel Dekker: New York, 1996, pp. 253–267.
[52] Barltrop JA, Coyle JD. *Excited States in Organic Chemistry*, Wiley-Interscience: New York, 1977.
[53] Ermolaev VL, Bodunov EN, Sveshnikova EB, Shakhverdov TA. Radiationless Electron Excitation Energy Transfer. Nauka, Leningrad, 1977.
[54] Kuhn H. Classical aspects of energy transfer in molecular systems. *J. Chem. Phys*. 1970, 53, 101–108.
[55] Lakowicz JR. *Principles of Fluorescence Spectroscopy*, 3rd ed., Springer: New York, 1983.
[56] Kubota Y, Steiner RF. Fluorescence decay and quantum yield characteristics of acridine orange and proflavine bound to DNA. *Biophys. Chem*. 1977, 6, 279–289.
[57] Harrington RE. Flow birefringence of persistence length deoxyribonucleic acid. Hydrodynamic properties, optical anisotropy, and hydration shell anistropy. *J. Am. Chem. Soc*. 1970, 92, 6957–6964.
[58] Navotny L, Hecht B. *Principles of Nano-Optics*, Cambridge University Press, Cambridge: New York, 2006.
[59] Förster W, Bauer E, Schütz H, Berg H, Akimenko NM, Minchenkova LE, Evdokimov YuM, Varshavsky YM. Thermodynamics and kinetics of the interaction of copper (II) ions with native DNA. *Biopolymers* 1979, 18, 625–661.
[60] Scheiber JP, Daune M. Interactions des ions métalliques avec le DNA. IV. Fixation de i'ion cuivrique sur le DNA. *Biopolymers* 1969, 8, 139–152.
[61] Voet D, Gratzer WB, Cox RA, Doty P. Absorption spectra of nucleotides, polynucleotides, and nucleic acids in the far ultraviolet. *Biopolymers* 1963, 1, 193–208.
[62] Cantor CR, Schimmel PR. Biophysical Chemistry, Part III. *The Behavior of Biological Macromolecules*. W.H. Freeman: San Francisco, 1980.
[63] Freese, EB. Molecular mechanism of mutation. In *Molecular genetics, Part 1*, Taylor JH, Ed., Academic Press: New York, London, 1963, 207–270.
[64] Drake JW. Spontaneous mutations accumulating in bacteriophage T4 in the complete absence of DNA replication. *Proc. Nat. Acad. Sci. USA* 1966, 55, 738–743.
[65] Danilov VS. Quantum chemical study of tautomery in nucleic acid bases and the problem of mutations. *Biofizika* 1967, 12, 540–544.
[66] Pullman B, Pullman A. La tautomérie des bases puriques et pyrimidiques et la théorie des mutations. *Biochem. Biophys. Acta* 1962, 64, 403–405.
[67] Pullman B, Pullman A. Electronic delocalization and biochemical evolution. *Nature* 1963, 196, 1137–1142.
[68] Pullman B. Adenine complexes of thymine and uracil. In *Electronic Aspects of Biochemistry*, Pullman B, Ed., Acad. Press: London, 1964, p. 135.
[69] Löwdin PO. Proton tunneling in DNA and its biological implications. *Rev. Mol. Phys*. 1963, 35, 724.
[70] Löwdin PO. Effects of proton tunneling in DNA on genetic information and problems of mutations, aiging and tumores. *Biopolym. Symp*. 1964, 1, 161, 293.
[71] Löwdin PO. Some aspects of DNA replication. Incorporation errors and proton transfer. In *Electronic Aspects of Biochemistry*, Pullman B, Ed., Acad. Press: London, 1964, p.167.
[72] Booij ML, Maund I, Clinton-Soeteman, van Oortmerssen AC. Fluorescence of acridine orange bound to DNA. *Histochemie* 1976, 21, 203–207.
[73] Zakharov SD, Ivanov AV, Wolf EB, Danilov VP, Murina TM, Nguen KT, Novikov EG, Panasenko NA, Perov SN, Skopinov SA, Timofeev PY. Structural rearrangements in the aqueous phase of cell suspensions and protein solutions induced by a light-oxygen effect, *Quantum Electron*. 2003, 33, 149–162.
[74] Yusupov AS, Zakharov SD. The laser-induced light-oxygen effect in oncological practice. *Creative Surg. Oncol* 2012, 2, 24–32, (in Russian).

Vasil Bregadze is a famous scientist in bio-molecular and bio-nanophysics, structure and functions of DNA, and metal effects on biological structures. He created a new methodological approach, which considers DNA as a model for such physical processes as proton and electron transfer, nonradiative transfer of electron excitation energy, and light re-emission that simplify the interpretation of the processes at DNA interactions with light, small molecules, and nanoparticles. Vasil is a Doctor of Physical and Mathematical Sciences (M. Lomonosov Moscow State University), Professor. He is the author of more than 100 scientific publications. He graduated from Moscow Institute of Physics and Technology. At present, he is Principal Scientist at Ivane Javakhishvili Tbilisi State University Andronikashvili Institute of Physics. The International Biographical Centre (Cambridge, UK) acknowledged him with the International Einstein Award for Scientific Achievements and the International Plato Award for Educational Achievements. In 2009, the same center acknowledged him as one of the 2000 Outstanding Scientists of 2009/2010. Vasil is a member of the American Chemical Society, the International EPR Society, and the International Society for Optical Engineering.

Tamar Giorgadze graduated from Ivane Javakhishvili Tbilisi State University from their Master Programme of Biological Expertise (Georgia). She is the author of seven scientific publications. She is a scientist in the Department of Biological Systems of Physics, Andronikashvili Institute of Physics. Currently, she is completing her PhD in the group led by Professor Vasil Bregadze. Her doctoral research is concerned with silver nanoparticle (AgNPs) interaction with the DNA macromolecule in various environmental conditions (ionic strength, dielectrically penetrability, temperature, and photo-irradiation) studied by spectrophotometric and spectrofluorimetric methods.

Zaza G. Melikishvili is principal scientist at the Department of Coherent Optics and Electronics, Chavchanidze Institute of Cybernetics of Georgian Technical University (IC GTU), Georgia. Before moving to IC GTU, he worked as a scientist at various institutions, including Prokhorov General Physics Institute, Russian Academy of Sciences (Russia), and Javakhishvili Tbilisi State University (Georgia). He holds the degree of candidate of Physical and Mathematical Sciences (equivalent to PhD) in Quantum Electronics. His current research focuses on quantum computation based on dynamics of spectroscopic transitions and optical/laser spectroscopy applications to medicine and biology.